

Complete Spatial Characterisation of N-glycosylation upon Striatal Neuroinflammation in the Rodent Brain

Ana Lúcia Rebelo

National University of Ireland Galway

Francesco Gubinelli

University of Paris Department of Medicine Paris Center: Universite de Paris UFR de Medecine de Paris Centre

Pauline Roost

University of Paris 5 Faculty of Medicine: Universite de Paris UFR de Medecine de Paris Centre

Caroline Jan

University of Paris Department of Medicine Paris Center: Universite de Paris UFR de Medecine de Paris Centre

Emmanuel Brouillet

University of Paris 5 Faculty of Medicine: Universite de Paris UFR de Medecine de Paris Centre

Nadja Van Camp

UCD Dublin: University College Dublin

Richard R. Drake

Medical University of South Carolina

Radka Saldova

NUI: National University of Ireland

Abhay Pandit (✉ abhay.pandit@nuigalway.ie)

NUI <https://orcid.org/0000-0002-6292-4933>

Research

Keywords:

Posted Date: February 23rd, 2021

DOI: <https://doi.org/10.21203/rs.3.rs-224054/v1>

License:   This work is licensed under a Creative Commons Attribution 4.0 International License.

[Read Full License](#)

Abstract

Background: Neuroinflammation is an underlying pathology of all neurological conditions, the understanding of which is still being comprehended. A specific molecular pathway that has been overlooked in neuroinflammation is glycosylation (i.e. post-translational addition of glycans to the protein structure). N- glycosylation is a specific type of glycosylation with a cardinal role in the central nervous system (CNS), which is highlighted by congenital glycosylation diseases that result in neuropathological symptoms such as epilepsy and mental retardation. Changes in N- glycosylation can ultimately affect glycoproteins' functions, which will have an impact on cell machinery. Therefore characterisation of N- glycosylation alterations in a neuroinflammatory scenario can provide a potential target for future therapies. **Methods:** With that aim, the unilateral intrastriatal injection of Lipopolysaccharide (LPS) in the adult rat brain was used as a model of neuroinflammation. In vivo and post-mortem, quantitative and spatial characterisation of both neuroinflammation and N- glycome was performed at one-week post-injection of LPS. These aspects were investigated through a multifaceted approach based on positron emission tomography (PET), quantitative histology, reverse transcription-quantitative polymerase chain reaction (RT-qPCR), liquid chromatography and matrix-assisted laser desorption ionisation mass spectrometry imaging (MALDI-MSI). **Results:** In the brain region showing LPS-induced neuroinflammation, a significant decrease in the abundance of sialylated and core fucosylated structures was seen (approximately 7.5% and 8.5%, respectively), whereas oligomannose N- glycans were significantly increased (13.5%). This was confirmed by MALDI-MSI, which provided a high-resolution spatial distribution of N- glycans allowing precise comparison between normal and diseased brain hemispheres. **Conclusions:** Together, our data show for the first time the complete profiling of N- glycomic changes in a well-characterised animal model of neuroinflammation. These data represent a pioneering step to identify critical targets that may modulate neuroinflammation in neurodegenerative diseases.

Background

Neuroinflammation is a complex pathology with multiple players that underlies most of the penetrating injuries (such as traumatic brain injury (TBI) and spinal cord injury (SCI)), and neurodegenerative conditions (such as Parkinson's disease (PD), Alzheimer's disease (AD), Multiple sclerosis (MS), and Amyotrophic lateral sclerosis (ALS) among others)¹⁻⁴. Neuroinflammatory cascades are mainly governed by glial cells, specifically microglia, which are the resident macrophages (immune cells) of the CNS. These, together with astrocytes and neurons, can trigger the complement system and express related receptors, being part of the innate immune system⁵⁻⁸. Additionally, upon neuronal insults, microglia become activated and start producing neurotoxic pro-inflammatory mediators such as chemokines (C-C motif chemokine ligand 2 (CCL2) or C-X-C motif chemokine ligand 10 (CXCL10)), cytokines (e.g. interleukin 1 β (IL-1 β), interleukin 6 (IL-6), tumour necrosis factor α (TNF α), interferon-gamma (IFN γ)), reactive oxygen species (ROS), nitric oxide (NO), prostaglandins and other secondary messengers⁹. If the blood-brain barrier (BBB) is compromised, peripheral immune and endothelial cells can infiltrate the CNS, exacerbating the inflammatory cascades¹⁰. The duration and extent of neuroinflammation will dictate

whether this will have a beneficial or detrimental outcome in the brain. Microglial activation is critical and necessary as a first-line in host defence due to phagocytosis and antigen presentation capability. However, chronic microglial activation can amplify inflammatory cascades, induce neuronal death, and feed into a degenerative after-effect¹⁰.

Lipopolysaccharide (LPS) is a potent immunostimulant that is naturally present in gram-negative bacteria's cell wall, which binds predominantly to Toll-like receptor 4 (TLR-4) abundantly present in microglia^{11,12} and, to a lesser extent, in neurons and astrocytes¹³⁻¹⁵. Upon TLR-4 activation, different downstream pathways are triggered in microglia (including NF- κ B and JAK-STAT cascades), ultimately leading to the activation of transcription factors and subsequent production of those mentioned above neurotoxic inflammatory factors^{16,17}. Administration of LPS in preclinical models induces, depending on the route of administration, behavioural impairments such as reduced locomotion, somnolence, memory deficiencies, decreased bodyweight, increased anxiety and general depression, amongst others, which are reminiscent of the clinical symptoms of neurodegenerative conditions like AD and PD¹⁸. Therefore, administration of LPS in rodents is well-established in the scientific community to model neuroinflammation-associated disorders [extensively reviewed by¹⁸⁻²⁰]. It has been widely used in mouse²¹⁻²³ and rat models^{19,24,25}, utilising distinct routes of administration, delivery methods, doses and timing of administration. Since its effect varies depending on the experimental design, experimental protocols are adapted to each study to achieve the optimal phenotype (acute vs chronic) with desired behavioural/cognitive outcomes. Moreover, LPS is also a powerful tool, both *in vitro* and *in vivo*, to further investigate the molecular and cellular mechanisms that take place upon neuroinflammation and test potential anti-inflammatory therapeutic strategies at the preclinical level²⁰.

A critical molecular aspect of neuroinflammation related to protein glycosylation has so far been overlooked. Proteins are fundamental players in any cell's structure and functions, including a plethora of signalling cascades, cellular architecture, matrix organisation, and biological interactions. Most proteins are post-translationally modified, with glycosylation being the most common of these modifications. Glycosylation consists of the addition of glycans (mono-, oligo- or polysaccharides) to a newly-formed peptide chain, regulating the structure and associated function of the final protein²⁶. This is a dynamic, flexible, non-template driven and highly variable process, which can change dramatically upon alterations within the cellular milieu²⁶. There are distinct glycosylation types in mammals that give rise to various glycoproteins categories such as *N*-linked, *O*-linked, GPI anchored or *O*-GlcNAc modified glycoproteins. The most abundant glycosylation class is the *N*-linked type since it has been reported that approximately 90% of eukaryotic glycoproteins carry *N*-glycans²⁷. *N*-glycosylation is a multifaceted biosynthetic mechanism that starts in the endoplasmic reticulum and is completed in the Golgi, regulated by glycosidases and glycosyltransferases that determine the arrangement of the different glycosidic chains^{28,29}. The knowledge about *N*-glycans' role in brain physiology is still limited; however, they are known to be involved in neuronal development and differentiation, synaptogenesis, and myelinogenesis³⁰. Nonetheless, the crucial role of *N*-glycans in the CNS is highlighted in the case of congenital disorders of glycosylation (CDGs), which result in multiple neuropathological symptoms that include epilepsy,

seizures, stroke-like episodes and developmental delays³¹. This emphasises the need for an in-depth characterisation of the brain *N*-glycome, specifically in neurological conditions such as neuroinflammation, to understand how glycosylation might be playing a role in the pathogenesis of brain illnesses.

In the past decade, interest has grown in the role of glycosylation in neuroinflammation and on how the glycomic profile might be altered in this condition, suggesting a possible target for future therapies³². Only a few *in vitro* studies have been performed so far; however, all of them consistently describe a decrease in sialylation in inflammation models^{33,34}. This reduction in sialylation was also seen in an LPS-injected post-natal rat model³⁵. Nonetheless, only perinatal infectious exposure was considered, and only one glycosylation trait was analysed (sialylation). This underlines the need and importance to evaluate neuroinflammation in the adult brain, covering the full *N*-glycome (as other glycosylation structures and features might play an essential role in this pathology).

Therefore, the aim of this study was to analyse the spatial modulation of the full *N*-glycomic profile in a rat model of neuroinflammation, using different glyco-analytical platforms such as liquid chromatography and mass spectrometry imaging. To establish a robust platform in which to characterise the *N*-glycome, we used a robust acute neuroinflammatory model induced by intrastriatal injection of LPS. Our results provide an insight into the glycosylation cues involved in inflammatory pathways (such as oligomannosylation, fucosylation and sialylation), and can help to identify targets to tackle it.

Methods

The study design is outlined in Figure 1. Briefly, the striatal neuroinflammation model was established by unilateral injection of LPS into the rat striatum (10 µg), and inflammation was confirmed one-week post-injection *in vivo* by positron emission tomography (PET) and then *post-mortem* through immunohistochemistry and gene expression of inflammatory markers (Figure 1a). At this time point, brains were also collected to perform an in-depth quantitative analysis of the striatal *N*-glycome through hydrophilic interaction ultra-performance liquid chromatography (HILIC-UPLC), which was then confirmed spatially by matrix-assisted laser desorption mass spectrometry imaging (MALDI-MSI) (Figure 1b). In all studies, the LPS-injected striatum was compared with the corresponding contralateral striatum to allow for a same-individual comparison.

Animals

Adult male Sprague-Dawley rats (Janvier, France) of 8 weeks of age weighing 300-350 g were used in this study. Animals were housed in groups of two per cage, on a 12 h light/12 h dark cycle, at 21–23 °C and humidity 50%, with food and water available *ad libitum* throughout the whole experiment. This study was carried out following European Union (Directive 2010/63/EEC) and French (Act Rural Code R214/87-131; authorisation no. B92-032-02) regulations and complied with Standards for Humane Care and Use of

Laboratory Animals of the Office of Laboratory Animal Welfare (OLAW – n°A5826-01). All surgical procedures were reviewed and approved by the local ethics committee and registered with the French Research Ministry of Education and Research (committee no. 44, approval no. 12-100, APAFIS no. 389-20150327162135690v02). All efforts were made to minimise animal suffering and animal care was supervised by veterinarians and animal technicians skilled in rodent healthcare and housing.

Surgeries

All surgical procedures were completed with animals under isoflurane anaesthesia ((Iso-Vet; Coumon d'Auvergne, France) in 100% O₂, followed by a mixture of ketamine (75 mg/kg) and xylazine (5 mg/kg). Once anaesthetised, animals were placed in the stereotactic frame and an intrastriatal injection of 2 µl of 5 µg/µL lipopolysaccharide (n=30, LPS, L2880, Sigma, France) diluted in 1x Dulbecco's Phosphate Buffer Saline (DPBS, Gibco) or PBS (n=12, 2 µl, supplementary figure S1a) was carried out. Injection coordinates were as follows³⁶: Tooth bar: - 3.3mm; Anterio-Posterior (basing on bregma): + 0.5 mm; Lateral (basing on bregma): ± 3 mm; Ventral (basing on dura): - 4.3 mm. The injection was achieved using an automatic pump (CMA-4004) with a speed of 0.5 µl/min, and a 34-gauge blunt-tipped needle connected by a polyethylene catheter to a 10 µL Hamilton syringe (Hamilton; Reno, USA). Once the infusion was completed, the needle was left in place for two minutes and then it was gently retracted.

Positron Emission Tomography (PET) imaging

In vivo PET imaging using [18F]DPA714 ([N,N-diethyl-2-(2-(4-(2-[18F]fluoroethoxy)phenyl)-5,7-dimethylpyrazolo[1, 5-a]pyrimidin-3-yl)acetamide] was performed on LPS injected animals to image the 18kD translocator protein (TSPO), a molecule located on the outer membrane of mitochondria, which is upregulated during inflammatory events³⁷. The radiochemical purity of [18F]DPA714 was greater than 99% and specific radioactivity ranging from 100 to 165 GBq/µmol. [18F]DPA714 was formulated in physiological saline, at an injectable volume between 1.0 to 1.5 mL and the dose of 61±13 MBq/mL (2.46±1.65 nmol/mL; mean ± SD).

According to PET image acquisition and reconstruction procedures, rats (n=9) were imaged seven days post-injection (dpi) as previously described³⁸. Briefly, animals anaesthetised under isoflurane anaesthesia (Iso-Vet; Coumon d'Auvergne, France; 1.5-2.5% in 100% O₂), and placed in a MicroPET® Focus 220 system (resolution: 1.5 × 1.5 × 1 mm; Siemens, France). A dynamic emission scan of 90 min was started simultaneously with the intravenous bolus injection of [18F]DPA714 (1 mL/min; Pump11 Elite, Harvard Apparatus Ltd.). The uptake of [18F]DPA714 was quantified by the non-displaceable binding potential (BP_{ND}) using a simplified quantification method (Ichise's non-invasive plot, MRTM0³⁹), based on (pseudo-) reference regions (in this study: the contralateral striatum). The analysis was performed using PMOD® software.

Tissue harvesting for immunohistochemistry

One week following LPS (or PBS, see supplementary figure S1) administration, and one day after PET imaging, animals were deeply anaesthetised by 4% isoflurane inhalation, followed by lethal injection of 180 mg/kg of sodium pentobarbital intraperitoneally. Depending on the analysis done, different procedures were followed for tissue processing. For immunohistochemistry analysis, animals were transcardially perfused with 280 mL of 4% paraformaldehyde (PFA) in 0.01 M phosphate-buffered saline (PBS). The brains were then collected, post-fixed for 24 h in 4% PFA at 4°C and transferred to 30% sucrose in PBS afterwards. These were cut into coronal sections of 40 µm using a freezing-stage microtome (CM1900, Leica, Germany). Striatal sections were kept at -20°C in antifreeze solution (made of 30% sucrose, 30% ethylene glycol in PBS) until use.

Immunohistochemistry

For free-floating immunohistochemistry (IHC), a previously established protocol was followed⁴⁰. Briefly, sections were washed in PBS three times for 10 min and then incubated for 20 min with 0.3% H₂O₂ in PBS (at room temperature (RT)). After washing the sections again in PBS three times for 10 min, sections were blocked in 4.5% normal goat serum (NGS) in PBS with 0.2% Triton™ X-100 (PBST). Afterwards, sections were incubated with primary antibody in 3% NGS in PBST overnight at 4°C. Primary antibodies used were: GFAP (1:10.000; Z0334; Dako), Iba1 (1:3.000, 019_19741; Wako) and Vimentin (1:2.000; IF01; Calbiochem). Sections were washed in PBS and incubated in appropriate biotinylated secondary antibody (1:1.000; Vector Labs) diluted in 3% NGS in PBST for one hour at RT, followed by one hour incubation in Vectastain ABC kit (Vector Labs). Staining was revealed using the DAB peroxidase substrate kit with nickel (Vector Labs); sections were then washed in PBS, mounted onto glass slides and allowed to dry overnight. On the following day, sections were dehydrated by consecutive immersions in a gradient of ethanol baths (50%, 70%, 96%, 100%) and cleared twice in xylene before sealing with a coverslip and Eukitt mounting medium.

Stained sections were imaged using an ImageScanner III (GE Healthcare, USA) with Epson scan software (Epson, USA). Image analysis was done using FIJI (ImageJ software, NIH, USA). Briefly, images were transformed into a binary mode (8-bit format). The scale was set, areas of interest were manually outlined for each section (including a blank region), and light intensity of interest areas was measured. Afterwards, staining intensity was calculated as optical density (after subtracting the background) according to the equation:

See equation 1 in the supplementary files.

Real-time quantitative PCR

For transcriptomic analysis, striata were dissected manually from the coronal 40 µm sections, using a surgical scalpel and a binocular microscope. mRNA was then extracted from these using E.Z.N.A.® FFPE RNA Kit (Omega Biotek, Georgia, USA) following the supplier's heat extraction guidelines. mRNA levels were measured using Nanodrop (Thermo Fischer Scientific), and their quality was validated using Bioanalyzer (Agilent). According to the manufacturer's instructions, mRNA was reverse-transcribed into cDNA using SuperScript™ VILO™ cDNA Synthesis Kit (Vilo Life Technologies).

RT-qPCR was performed using iTaq™ Universal SYBR® Green Supermix (Bio-Rad) and primers (Eurofin Genomics) specific to different targets on 0.35-1 ng of cDNA, using 10 nM of primers (see Table 1). Reactions were run in triplicates in 384-well PCR plates, using a mix of cDNA and a housekeeping gene primer as an inter-plate control. Data were analysed using Bio-Rad CFX Maestro software (Bio-Rad). Cycle threshold (Ct) values were generated in regression mode. Results are shown as relative normalised expression.

Table 1: List of primers used for RT-qPCR

Gene/Primer	Forward sequence	Reverse sequence
Ppia / Cyclo (housekeeping)	ATGGCAAATGCTGGACCAAA	GCCTTCTTTCACCTTCCCAA
Rplp0 (housekeeping)	CAGGCGTCCTCATTAGAG	ATCTGCTGCATCTGCTTGGAG
Hprt1 (housekeeping)	GGACCTCTCGAAGTGTGGATAC	CCCTGAAGTGCTCATTATAGTCAA
GFAP	AATGACTATCGCCGCAAC	CTCCTGGTAACTCGCCGACT
IBA1	CCAGCCTAAGACAACCAGCGTC	GCTGTATTTGGGATCATCGAGGAA
TNFα	AAATGGGCTCCCTCTCATCAGTTC	TCTGCTTGGTGGTTTGCTACGAC
TSPO / PBR	CAGTGTCCCTTACGGAGCAG	CGGGTACCCAGGATTGAGAC
Vimentin	GCAAAGCAGGAGTCAAACGA	AATTCTCTTCCATTTACGCATCT

Tissue extraction and homogenisation for *N*-glycome analysis

For *N*-glycome analysis through liquid chromatography-based methods, snap-frozen tissue was used. Intact brains were collected as previously mentioned and mounted onto a cryostat chuck using optimal cutting temperature compound (OCT; Sigma, Ireland) and fully sectioned into 200 µm slices in a Microm HM 505 E cryostat (GMI; USA). These were collected on SuperFrost™ Plus Adhesion charged slides (Fischer Scientific, Ireland) where it was easier to identify the sections containing striatum using a rat brain atlas. To isolate and extract these regions, micron biopsy punches of 2 mm and 0.5 mm in diameter (Harvard apparatus; USA) were used. This procedure was carried out entirely inside the cryostat, at -20 °C. Striatal tissue punches were collected, weighed and stored at -80 °C until being processed further.

The snap-frozen striatal tissue was homogenised in RIPA buffer (Sigma, Ireland) and cOmplete Protease Inhibitor Cocktail (Roche, Ireland, 1:25) using the Qiagen TissueLyser LT (Qiagen, UK), during 8 minutes at 40 Hz (at 4 °C). The homogenates were centrifuged for 20 minutes at 16.000 g (4°C) and the supernatants collected and kept at -80 °C until further use.

N-glycan analysis by liquid chromatography

a. Materials and Reagents

For *N*-glycan release and analysis by liquid chromatography, the following materials and reagents were used. AcroPrep Advance 96-filter plates and 10 kDa MWCO microcentrifuge filtration tubes were acquired from Pall Life sciences (US). Polypropylene 2 mL deep 96-well blocks were purchased from Fisher Scientific (Ireland) and 0.45 µm Millex-LH filters from Millipore (Ireland). Plate seals were obtained from Cruinn (Ireland) and silicone sealing mats from Phenomenex (Germany). Protogel was purchased from National Diagnostics (UK) and ammonium hydroxide solution was acquired from Fluka (Ireland). Formic acid and ammonium persulfate (APS) were obtained from VWR chemicals (Ireland). Ultrapure water was filtered through an arium® ProUV system (Sartorius, Germany). HPLC grade methanol, ethanol, acetonitrile, xylene and water were acquired from Fisher Scientific (Ireland). PNGase F was purchased from New England Biolabs. All other reagents were purchased from Sigma (including N,N,N',N'-tetramethylethane-1,2-diamine (TEMED), iodoacetamide (IAA), dithiothreitol (DTT) and 2-aminobenzamide (2-AB)) unless otherwise specified.

b. Release of N-glycans

The isolated glycoproteins from brain tissue were dried in a vacuum centrifuge overnight (Savant™ SPD131DDA SpeedVac™ Concentrator, Fisher, Ireland) and *N*-glycans released from dried tissue as described previously⁴¹. Briefly, the glycoproteins were dissolved and then immobilised in acrylamide gels made of protogel and sodium dodecyl sulfate (SDS). The gels were cut and washed, followed by reduction and alkylation of the proteins with DTT and IAA, respectively, in 96-well plates. This allowed for the disulphide bonds from the protein to be disrupted, exposing *N*-glycan residues. *N*-glycans were cleaved using *N*-glycanase PNGase F (1239U/ml, New England BioLabs, Inc., UK)⁴².

c. 2-AB labelling of N-glycans

Released *N*-glycans were fluorescently labelled with 2-aminobenzamide (2-AB) by reductive amination^{43,44}. Briefly, the 2-AB labelling solution containing sodium cyanoborohydride was added to the glycans and incubated at 65 °C for two hours. The excess 2-AB solution was removed by absorption on Whatman 3MM paper (Merck, Ireland) in acetonitrile washes, being the final glycans eluted in water⁴⁵.

d. Hydrophilic interaction liquid chromatography ultra-performance liquid chromatography (HILIC-UPLC)

Labelled *N*-glycans were analysed by hydrophilic interaction liquid chromatography ultra-performance liquid chromatography (HILIC-UPLC). This was carried out using a UPLC Glycan BEH Amide Column, 130A, 2.1 x 150mm, 1.7 µm particles (Waters, USA) on an H Class Acquity UPLC system (Waters, USA) assembled with a Waters Acquity fluorescence detector and a Waters temperature control module. This was used to keep the column temperature at 40 °C and the sample temperature at 5 °C. Solvents A (50 mM ammonium formate, pH 4.4) and B (acetonitrile) were used in a method that had a duration of 30 minutes. The method consisted of a linear gradient of 30% to 47% of solvent A for 24 minutes at 0.561 mL/min flow rate, increasing to 70% at minute 25 and returning to 30% at minute 27 until the end of the run. Samples were suspended and injected in 70% acetonitrile. Once in the system, these were excited at 330 nm and fluorescence recorded at 420 nm. The instrument's internal calibration was done at the beginning of each sample set using a dextran ladder of 2-AB-labelled glucose oligomers (Water, USA) as previously described⁴⁴.

Tissue processing for MALDI-MSI

For *N*-glycome analysis through mass spectrometry imaging, frozen 10 µm serial sections of brain tissue on SuperFrost™ Plus Adhesion charged slides (Fischer Scientific, Ireland) were used. However, these had to be transformed before being used for imaging. Briefly, sections were thawed for 15 minutes and dehydrated in serial dilutions of ethanol (70%, 90%, 100%, 100%) for two minutes each. Afterwards, sections were incubated at 60 °C for 50 minutes, followed by delipidation in Carnoy solution twice (60% ethanol, 30% chloroform, 10% glacial acetic acid), for three minutes, and two minutes wash in running tap water. Finally, these were incubated for 30 minutes with 10% formalin solution, neutral buffered (Sigma, Ireland) at room temperature, followed by two washes in tap water. The samples were then air-dried and kept at room temperature in a desiccator until further analysis.

N-glycan analysis by MALDI-MSI

a. Antigen retrieval

The previously transformed slides were subjected to antigen retrieval using citraconic anhydride buffer (ThermoScientific™, USA), prepared by mixing 25 µL of citraconic anhydride in 50 mL of HPLC grade water, adjusted to pH 3 with 12 M HCl. Slides were incubated in this buffer for 30 minutes in a vegetable steamer (around 95 °C) and then washed (after cooling) in serial dilutions of the buffer by replacing half of the buffer with HPLC grade water, three times, eventually replacing it entirely with water. The slides were desiccated and scanned before applying PNGase F.

b. Application of PNGase F and CHCA matrix

After antigen retrieval, slides were coated with 0.25 mL aqueous solution of recombinant PNGaseF (Bulldog Bio, USA) at 0.1 µg/ µL, spraying at 25 µL/min in 15 passes at 45 °C, using an HTX™-Sprayer

(HTX Imaging, USA) as previously described⁴⁶. This was followed by an incubation of two hours at 37 °C in a humidified chamber and placed in the desiccator until sprayed with matrix (ideally on the same day). α -Cyano-4-hydroxycinnamic acid (CHCA) matrix was prepared fresh (7 mg/mL in 50% acetonitrile 0.1% TFA) and applied in the sections at 100 μ L/ min in 10 passes at 0.1 mL/min at 80 °C using an HTX TM-Sprayer (HTX Imaging, USA). Coated slides were stored in a desiccator until analysed.

c. MALDI-MSI analysis set up

Released *N*-glycan ions were detected using a MALDI timsTOF Flex trapped ion mobility separated QTOF mass spectrometer (Bruker Daltonics, Germany) operating in a positive mode as described by McDowdell et al.⁴⁷. This had a SmartBeam 3D laser operating at 10 kHz and a laser spot size of 20 μ m. Signal was collected at a raster width of 40 μ m between spots. A total of 300 laser shots were collected to form each pixel. Following acquisition, data was processed, and images of expressed glycans were generated using FlexImaging 5.0 and SCiLS Lab 2017b software (Bruker Daltonics, Germany), where ions in the range of 500-4000 *m/z* were analysed. Observed mass/charge ratios (*N*-glycans) were searched against glycan databases using GlycoWorkbench. Represented glycan structures were also generated in GlycoWorkbench, as they were determined by a combination of their measured accurate *m/z*, CID fragmentation patterns and previous structural characterisation carried out by UPLC (as described previously).

Glycan nomenclature

N-glycans share a common pentasaccharide with two core *N*-Acetylglucosamine (GlcNAc) and three mannose residues. F indicates a fucose residue, so if it is placed at the start of the abbreviation, it refers to core $\alpha(1,6)$ -fucose linked to the inner GlcNAc, whereas if it appears anywhere else, it indicates an outer arm $\alpha(1,3)$ or $\alpha(1,4)$ -fucose linked to antenna or galactose. Ax indicates the number (x) of antenna (GlcNAc) on the mannose residues belonging to the *N*-glycan core. Gx refers to the number (x) of $\beta(1,4)$ -linked galactose on the antenna and Galx to the number (x) of $\alpha(1,3/4/6)$ -linked galactose on $\beta(1,4)$ -linked galactose. Sx relates to the number (x) of $\alpha(2,3/6/8)$ -linked neuraminic acids (sialic acids) connected to galactose, while Sgx stands for the number (x) of glycolylneuraminic acids linked to galactose. Mx refers to the number (x) of mannose residues on the core GlcNAc (terminology used in oligomannose glycans). Lacs concerns the number (x) of poly-*N*-Acetylglucosamine repeats consisting of GlcNAc $\beta(1,4)$ -linked to galactose.

Statistical analysis

Data were processed using GraphPad Prism8 software. Immuno-histochemistry data, qPCR data and PET imaging data are expressed as mean \pm SEM. These were analysed using paired Student's t-test to compare LPS-injected and non-injected (NI)/contralateral striata in the same animal. *N*-glycome data was also analysed using paired Student's t-test, after Log- transforming each glycan peak's abundance to

obtain a normal distribution. The statistical significant difference was set at * $p < 0.05$, ** $p < 0.01$, *** $p < 0.001$, **** $p < 0.0001$, and significance is expressed between glycosylation levels in LPS-injected striatum vs NI striatum. n indicates the number of rats.

Results

LPS-injected striatum displays neuroinflammatory hallmarks *in vivo* and *post-mortem*

To establish a robust platform in which to characterize the N -glycome, a rat model of striatal neuroinflammation was optimised (Figure 2). *In vivo* PET imaging of the 18kD TSPO showed a statistically significant increased BP_{ND} in the LPS-injected striatum compared to the non-injected (NI) contralateral side (Figure 2a & 2b, b, $n=9$, Paired Student's t-test, $p < 0.0011$). This was correlated with the TSPO mRNA expression, where a significant increase was also detected by RT-qPCR in the LPS-injected side (Figure 2c, $n=11$, $R = 0.87$, Paired Student's t-test, $p < 0.0004$).

In vivo data was correlated with *post-mortem* data correlated through Spearman correlation analysis, showing positive associations between all different inflammation-related markers (Figure 2d), between 0.74 (GFAP mRNA expression vs TSPO BP_{ND}) and 0.85 (Vim mRNA expression vs TSPO BP_{ND}).

Post-mortem analysis of inflammatory markers [glial fibrillary acid protein (GFAP), ionised calcium-binding adapter molecule 1 (Iba-1) and vimentin (Vim)], both by mRNA expression through RT-qPCR (Figure 2c) and by IHC analysis (Figure 2e-j) confirmed LPS induced localised neuroinflammatory reaction. The density of activated microglia, as detected by IHC of the protein Iba1, was significantly increased in the LPS-injected striatum as compared to NI control striatum ($+322 \pm 25\%$, $n=12$, Paired Student's t-test, $p < 0.0001$) (Figure 2e & 2h). In parallel, increased presence of astrocytes (GFAP and Vim) was observed in the LPS-injected striatum compared to the NI striatum [GFAP IHC ($+107 \pm 11\%$, $n=12$, Paired Student's t-test, $p < 0.0001$) (Figure 2f & 2i); and vim IHC ($+544 \pm 238\%$, $n=12$, Paired Student's t-test, $p < 0.0001$) (Figure 2g & 2j)]. These results were coherent with the mRNA expression data (Figure 2c) for each of these markers, where a dramatic increase of Iba1 ($+371\%$, $n=11$, Paired Student's t-test, $p < 0.0001$), of GFAP ($+181\%$, $n=10$, Paired Student's t-test, $p < 0.0001$) and of vimentin ($+454\%$, $n=10$, Paired Student's t-test, $p = 0.0002$) was seen. Additionally, mRNA expression of the pro-inflammatory cytokine Tumour necrosis factor α (TNF α) was also significantly increased in the ipsilateral striatum ($+277\%$, $n=10$, Paired Student's t-test, $p = 0.0003$).

To confirm that LPS was responsible for the neuroinflammatory reaction, a parallel study was done on a subgroup of PBS-injected animals (Supplementary figure S1a). Immunohistological analysis in the PBS-injected striatum of the inflammatory markers (Iba1, GFAP, Vim) did not show any significant increase in the density of any of these markers as compared to the NI striatum (Figure S1c-h) [Iba1: $n=6$, Paired Student's t-test, non-significant (NS); GFAP: $n=6$, Paired Student's t-test, NS; Vim, $n=5$, Paired Student's t-test, NS]. mRNA expression of Iba1 and GFAP was also not altered in the PBS-injected striatum compared

to contralateral NI side (Figure S1b; Iba1: NS, n=7, Paired Student's t-test; GFAP: NS, n=6, Paired Student's t-test). The expression of TNF α mRNA was increased in the PBS-injected striatum compared to contralateral NI side (Figure S1b; n=6, Paired Student's t-test, p=0.0071). However, the expression of TNF α after PBS injection was lower than the LPS-injected striatum (TNF α mRNA expression was 25% higher in the LPS-injected striatum in comparison to the PBS-injected striatum). Altogether, these data confirmed that LPS induces a significant neuroinflammatory reaction, providing a robust and reproducible model.

***N*-glycome profile in the LPS-injected striatum is significantly different from that in the contralateral (non-injected) hemisphere**

To quantitatively analyse the changes in *N*-glycome seen in the LPS-injected striatum, hydrophilic interaction liquid chromatography ultra-performance liquid chromatography (HILIC-UPLC) was used as previously described⁴¹. This provided the *N*-glycans' chromatographic profile isolated from the glycoproteins present in the LPS-injected and NI striata, after releasing them using PNGase F and labelling them with 2-AB (Figure 3). Chromatograms of 26 glycan peaks (GP) were observed (Figure 3a, Supplementary table S1). When pooled into the main biosynthetic classes, there is a decrease in complex structures and an increase in oligomannose, as would be predictable from the individual GPs changes (Figure 3b).

From the 16 GPs identified, 16 of them were significantly different between LPS-injected and NI striata (Figure 3c). From these, nine were significantly increased following LPS injection, mainly oligomannosylated structures (Figure 3c, M3: n=5, Paired Student's t-test, p<0.0009; M3B: n=5, Paired Student's t-test, p<0.0004; M8: n=5, Paired Student's t-test, p<0.02; M9: n=5, Paired Student's t-test, p<0.0016). The GPs significantly decreased were mainly sialylated (Figure 3c, A2G2S1Ac: n=5, Paired Student's t-test, p<0.0161; A2G2S2: n=5, Paired Student's t-test, p<0.0057; FA4F3G4S1: n=5, Paired Student's t-test, p<0.0001).

Looking in greater depth into the main glycosylation features, GPs were grouped into traits such as sialylation, core fucosylation, outer-arm fucosylation, branching degree and bisected *N*-glycans (Figure 4) following the calculation rationale described in Supplementary table S3. It was seen that in all of these there were significant differences: a drastic decrease in sialylation (n=5, Paired Student's t-test, p<0.0005), in core fucosylation (n=5, Paired Student's t-test, p<0.0044), in outer-arm fucosylation (n=5, Paired Student's t-test, p<0.0131) and in structures with 2, 3 or 4 antennae (or bisecting monoantennary, bisecting diantennary or bisecting triantennary, respectively) (A2/A1B: n=5, Paired Student's t-test, p<0.0405; A3/A2B: n=5, Paired Student's t-test, p<0.0001; A4/A3B: n=5, Paired Student's t-test, p<0.0001) were seen after LPS injection. In contrast, there was a significant increase in oligomannose structures (n=5, Paired Student's t-test, p<0.0021) and in bisected *N*-glycans (n=5, Paired Student's t-test, p<0.0002).

Sialylation and Fucosylation are the main traits dysregulated upon neuroinflammation

General discrepancies in sialylation and fucosylation have been reported in CNS-impairments and neuroinflammatory scenarios^{35,48}. Therefore, we looked further into these two features in the context of *N*-glycosylation (Figure 5). Regarding fucosylation, a decrease was seen in both outer arms and core fucosylation, as mentioned above (Figure 5a). However, the main structures affected were the heavily fucosylated ones (with four fucose residues – F4; n=5, Paired Student's t-test, p<0.0001) (Figure 5b). Interestingly, in the case of sialylation, the decrease seen in the LPS-injected group seems to be due to a lower abundance in mono-sialylated *N*-glycans (n=5, Paired Student's t-test, p<0.0001) (Figure 5c). Additionally, the primary type of linkages affected is the α 2,3 (n=5, Paired Student's t-test, p<0.0001), whereas sialic acid bound through α 2,6 linkages seems to remain unaffected (Figure 5d).

Spatial distribution of *N*-glycome in LPS injected striatum is region-dependent

To elucidate the spatial distribution of the brain *N*-glycophenotype upon LPS injection, MALDI-MSI of *N*-glycans was used as described by Powers et al.⁴⁹. In this case, fixed-frozen tissue sections were used, and, after antigen retrieval, sections were sprayed with PNGaseF, followed by α -Cyano-4-hydroxycinnamic acid (CHCA matrix) to facilitate ion detection. The glycan composition analysis was performed by identifying the mass to charge ratio of each peak and comparing it to a database in GlycoWorkBench with all possible mammalian *N*-glycan compositions. These were further compared with the databases from the Consortium for Functional Glycomics (www.functionalglycomics.org) for comparison with previous studies and discard any biologically irrelevant matches. This promoted the validation of the data previously detected by HILIC-UPLC and further refinement and in-depth elucidation of the rodent striatum's *N*-glycome. An intra-animal comparison was performed to follow the analysis done previously.

Overall, a total of 52 *N*-glycans were detected by MALDI-MSI (panels of all detected *N*-glycans through MALDI-MSI are described in Supplementary Figure S2, Supplementary Figure S4, Supplementary Figure S5 and Supplementary table S2), providing a high-resolution spatial distribution of *N*-glycans in the rodent striatum. There are some dramatic changes seen in the injection site, directly correlated with the inflammatory reaction (Figure 6). These changes are mainly characterised by the marked increase in the expression of oligomannose, bisected and α -galactosylated structures in the lesion core (i.e. in the striatum, and across the needle tract in the cortex).

On the other hand, some structures seem to be depleted upon neuroinflammation, not only in the striatum but in the whole hemisphere (including the cortex, where no signs of inflammation are seen – data not shown). Overall, these include the fucosylated and sialylated structures, which seem to be down-regulated in the LPS-injected side (Supplementary Figure S4), following the UPLC data trends. Regarding the 16 glycan structures whose abundance was seen to be significantly different between LPS-injected

and NI striata, 10 of them were detected by MALDI-MSI (Supplementary Figure S3). Five out of the six non-detected structures are sialylated; however, due to the low abundance and instability of sialic acids, which can be readily lost in MSI steps^{50,51}, both in the ion source and during the flight to the detectors, this would be expected. The detected GP's spectra were plotted according to their intensity in each striata, and it was seen that the trends in intensity (LPS-injected vs NI striata) are similar to the significant changes indicated by HILIC-UPLC (Supplementary Figure S3).

Discussion

N-glycosylation is a type of post-translational modification whose dysregulation in the brain dictates many conditions ultimately related to neuronal dysfunction^{52,53}. However, the *N*-glycophenotype of distinct neurological scenarios is still unknown, representing a gap in the in-depth knowledge of such diseases. To date, this is the first study to explore the complete modulation of the *N*-glycome upon neuroinflammation in the rodent brain. It was hypothesised that the spatial distribution of *N*-glycans in the striatum of a rodent model of neuroinflammation gives an insight into the glycosylation cues involved in the inflammatory pathways and identify potential targets to tackle it. To test this hypothesis, firstly an *in vivo* acute model of neuroinflammation was optimised to ensure reproducibility of the lesion and consistency in the results. This was followed by quantitative analysis of the changes in the expression of different *N*-glycan structures between LPS-injected and non-injected striata, which was finally validated spatially by assessing the distribution of the *N*-glycome in the brain of this preclinical model, using different glyco-analytical platforms such as HILIC-UPLC and MALDI-MSI. This follows a previous study by our group where the detailed and specific *N*-glycosylation profiles of the rat striatum and substantia nigra were comprehensively characterised⁴¹.

A multifaceted approach combining *in vivo* and *post-mortem* tools on the same animals was undertaken to measure inflammatory-related markers in the ipsilateral striatum to characterise the neuroinflammation model. Significantly increased TSPO binding *in vivo* using [18F]DPA714 PET imaging was seen in the LPS-injected striatum, which most likely is related to an increased density of LPS-induced pro-inflammatory TSPO-expressing microglia. This was previously suggested in a mouse model where the expression of TSPO was significantly increased upon microglial activation after peripheral LPS administration^{54,55}. However, also activated astrocytes contribute to the [18F]DPA714 TSPO-PET signal³⁸, and as such, it is most likely that both cell populations are actively contributing to the TSPO-PET signal. *Post-mortem* analysis of the tissues through immunohistochemistry confirmed the significantly higher density of microglia and reactive astrocytes and confirmed their morphological changes typical of a reactive phenotype. This is in coherence with previous studies demonstrating that LPS-induced pro-inflammatory microglia can induce astrocytes activation⁵⁶. In our study, we were able to see that astrocytes are significantly more expressed in an acute neuroinflammation model, even if at a lower abundance than that of microglia. Additionally, there is a strong association between the expression of TSPO and GFAP/Vimentin (astrocytic markers), highlighting the correlation between them.

Another crucial hallmark of neuroinflammation in addition to increased microglial density is the secretion of pro-inflammatory cytokines and other neurotoxic factors⁵⁷, which have a deleterious effect on the neuronal circuitry⁵⁸. This neuronal damage feeds further into a positive feedback loop, which promotes further inflammation. Our results show a significant increase in the production of TNF α post-LPS-injection that can be mainly secreted by microglia and infiltrating macrophages, which express CD68⁵⁹. This supports the previous reports, such as the LPS model established by Ory and colleagues, which was described to increase CD68+ cells significantly in the LPS-injected striatum⁶⁰. Beier et al. also showed an increase in activated microglia and CD68+ cells in the brain after systemic and repeated injection of LPS⁶¹. Additionally, the model implemented by Herrera et al. showed an increase in integrin alpha M (ITGAM)-positive cells with macrophage morphology in the core of the lesion⁶², also corroborating what we described and emphasising that the PET signal seen is most likely due to microglia/macrophages contribution. These results confirm the establishment of a robust acute neuroinflammatory model that with a moderate dose of LPS (10 μ g) can induce high expression of reactive astrocytes and microglia and other inflammatory markers such as TNF α and TSPO.

The effect of glycosylation in inflammatory cascades and how this is modulated during the different neuroinflammation phases has been of increased research interest in recent years. A clear example comes from the pro-inflammatory activity of TNF α , which is predominantly mediated by TNF receptor 1 (TNFR1), whose *N*-glycosylation was reported to be altered in microglia⁶³. This facilitates the interaction and increases binding-affinity of TNF α to this receptor, promoting further an autocrine loop in microglia and increasing the inflammatory cascades.

Having established a reproducible neuroinflammation model, it was possible to use it to investigate the modulation of tissue *N*-glycosylation in this scenario. Even though some *in vitro* studies were conducted in different models to investigate glycan changes, most of these studies explore only specific glycosylation traits (e.g. sialylation), or are not focused on a type of glycosylation (such as *N*-glycans or *O*-glycans), but rather on the overall glycomic signature. To date, only one *in vivo* study was carried out to explore a single glycosylation trait in a model of neuroinflammation³⁵, leaving a gap in this knowledge. Furthermore, studying the *N*-glycome of the overall tissue instead of specific glycoproteins offers the advantage of promoting therapeutic approaches that can attenuate these global dysregulations, rather than targeting individual molecules, which is exponentially more complex.

Looking at the modulation of the overall *N*-glycosylation traits upon LPS-injection, the decrease in sialylation comes as an interesting and expected result. Sialic acids are crucial players in CNS homeostasis, axonal guidance and neuronal growth^{64,65}, mainly for their polarisation (negative charge). They modulate the voltage-gated ion channels (VGICs) activity in an isoform-specific manner according to the cell type, environment, and developmental stage⁶⁶. This residue's importance is probably why most glyco-targeted studies in the brain are focused on sialylation. For example, it was seen that mice deficient in sialyltransferases St3gal2 and St3gal3 (mainly involved in the assembly of gangliosides) presented motor impairments and cognitive deficits, besides increased dysmyelination⁶⁷, indicating the

crucial role of sialylation. As LPS impacts microglia, which modulates neuronal function and synaptic maintenance, a decrease in sialylation could be involved in the dysregulation of signal transmission. Sumida et al. reported that LPS-activated microglia display upregulated secretion of a sialidase (NEU1) that cleaves polysialic acid (PSA) in neural cells³⁴, which comes in line with the decrease in sialylation that we found in the present study. This suggests that the increase seen in the abundance of microglia and its reactivity could be involved with decreased sialylation through the elevated secretion of sialidases (enzymes responsible for cleaving sialic acid residues)⁶⁸ or decreased secretion of sialyltransferases. Similar findings were seen *in vivo*, in a post-natal neuroinflammatory model (LPS injected), where a significant upregulation in sialidases was described, leading to decreased sialylation³⁵.

In an *in vitro* model where reactive astrocytes and neurons were used, it was reported that α 2,6-sialic acid is absent in the healthy neuronal culture, but present in neurons in the injured environment. This indicates that changes in sialylation might be a consequence of the injury and that sialic acid could be contributing to the pathology⁶⁹. The low abundance of α 2,6-sialic acid in the striatum revealed no significant differences in our study, which might suggest that in a complex *in vivo* environment, these do not play such a crucial role. On the other hand, it has been reported that *N*-glycans in the adult brain display predominantly α 2,3-linked sialic acids^{52,70,71}, which is consistent with what we have described. The significant decrease in this structure upon LPS-injection might be related to dysmyelination and neuronal impairment, as α 2,3-linked sialic acids have been reported to be essential players in these physiological functions⁵²; however, further studies would be required to assess if our model presents dysmyelination.

The presence of structures containing polysialic acids (PSA) is also of interest as these are almost exclusive of neural cell adhesion molecule (NCAM), linked through α 2,8 linkages, appearing also associated to voltage-dependent sodium channels⁵². Thus, these are pivotal for neural cell interactions, brain plasticity and development^{52,72,73}. We saw that PSA expression in the rodent striatum was very low (around 5%), as reported by Samal et al.⁴¹. However, upon LPS-injection, only the expression of one polysialylated structure was significantly increased, but in a very low abundance, indicating that it is not so much involved in neuroinflammatory signalling. A similar trend in upregulation of PSA-NCAM was seen in a Parkinsonian rat model (after injection of 6-hydroxydopamine to trigger neurodegeneration) as a marker for reactive astrocytes only at the site of lesion⁷⁴. This corroborates the hypothesis that modulation of PSA's presence in the brain is associated with the reactivity and proliferation of resident cells and is upregulated in regions of high neuronal plasticity⁷⁵. The increase in reactive astrocytes seen in our study at the injection site might be correlated with the increase seen in polysialylated structures.

Besides sialylation, fucosylation is another pivotal glycosylation trait in the brain⁷⁶ since it regulates neurite outgrowth and synaptic plasticity, being crucial for cognitive processes [reviewed by Schneider et al.⁷⁷]. This would be expected as an abundant distribution of fucosylated *N*-glycans was reported in the rodent brain⁴¹, being higher than that in other mammalian tissues⁷⁶.

The cardinal role of core fucosylation in regulating neuronal functions is highlighted in a study by Fukuda et al., where mice lacking α 1,6-fucosyltransferase (Fut8 – an enzyme responsible for the attachment of a fucose residue to the core pentasaccharide characteristic of *N*-glycans) display behavioural impairments and schizophrenia-like behaviour⁷⁸. This loss of Fut8 was later reported to decrease long-term potentiation in the hippocampus, impacting neuronal synaptic plasticity and, subsequently, learning and memory⁷⁹. This accounts for the schizophrenia-like phenotype seen in the animals lacking this enzyme⁷⁹. It has been reported that deficiency of α 1,6-fucosyltransferase has a deleterious impact on glial cells (both astrocytes and microglia, in addition to the effect seen in neuronal cells), promoting their sensitivity to inflammatory mediators⁴⁸. This might suggest that our LPS model (with an increase in reactive glial cells) impacts the production of Fut8, downregulating its expression, which contributes to a lower abundance of core fucosylated *N*-glycans. This feeds further into a positive loop that reinforces the neuroinflammatory cascades. However, further studies on this enzyme's expression will be required to confirm such hypothesis.

Regarding outer arm fucosylation, Kalovidouris et al. have shown that Fuc α 1,2-Gal residues play a role in neuronal outgrowth and morphology, influencing long-term memory⁸⁰. Additionally, outer arm fucosylation is also particularly important in the formation of Lewis^X epitopes (trisaccharide composed of Gal β 1-4 (Fuc α 1-3) GlcNAc)⁸¹ and Sialyl-Lewis^X epitopes (Lewis^X epitope with a Neu5Ac residue attached to it), which are known to be central for brain development^{82,83}. A decrease in Lewis^X structures due to the absence of α 1,3-fucosyltransferase IX (Fut9) was described to induce anxiety-like behaviour in mice^{81,84}. The results seen in our LPS model come in accordance to this, since there is a decrease in the abundance of both *N*-glycans with Lewis^X epitopes and with Sialyl-Lewis^X epitopes, indicating that their absence might be contributing to the pathological condition, which might be both an effect as well as a cause of inflammatory cascades, participating in a cyclic chain of events.

Oligomannose structures are also essential players in neuroinflammatory processes due to the expression of mannose-binding lectins in astrocytes and microglia, which control immune responses through the lectin pathway of complement activation⁸⁵. An increase in oligomannose *N*-glycans upregulates the binding to these receptors and, consequently, triggers the complement response, promoting further inflammation. This accords with our findings, since there is a significant increase in microglial activation and oligomannose structures, indicating the crosstalk between glycosylation and neuroinflammation. Nonetheless, additional studies on the expression of these lectins and other carbohydrate-binding proteins would be needed to confirm their influence in this condition.

The results seen through HILIC-UPLC were reinforced by MALDI MSI, with the added advantage of spatially characterising each glycan structure's distribution. The expected increased expression of oligomannose and bisected glycans in the LPS-injected striatum was seen, as well as a decrease in fucosylated *N*-glycans in the overall hemisphere. Additionally, MALDI MSI allowed for the detection of specific structures that were not distinguished by HILIC-UPLC since only the major glycan constituent of each peak was considered for this latter analysis. This comes as a disadvantage in HILIC-UPLC since if

each chromatogram peak corresponds to more than one glycan, then the ones in lower abundance will not be considered, resulting in an incomplete detection of some traits. Nevertheless, by combining it with *N*-glycans' MALDI imaging, it is possible to have a complete characterization of the *N*-glycome modulation upon neuroinflammation. This is of interest since it shows that *N*-glycans can be directly detected on tissue sections with high sensitivity and specificity.

It appears that there are specific structures that are dramatically increased upon inflammation, being characteristic of this event and promoted by it. In contrast, others seem to be significantly decreased in the whole hemisphere, suggesting a posterior effect of LPS/neuroinflammation at the *N*-glycome level and on such structures' biosynthesis.

An aspect worth noting in this technique relates to the technical challenges in detecting sialic acids that were common during the past decades. Due to their instability, these can be easily lost in MSI steps, which decreases their detection^{50,51}. This can be circumvented by fragmentation of derivatised glycans to increase sialic acid stabilisation^{50,86,87}, which can be addressed by the new instrumentation's advances. Nonetheless, following the results acquired by HILIC-UPLC, it seems that the abundance of sialic acids in the brain is overall reduced. Therefore, a low detection of sialic acid was expected. This low detection of sialic acids in the brain through MALDI imaging was also seen in a previous study where *N*-glycans from a mouse brain were analysed through MALDI quadrupole ion trap (QIT) time of flight (ToF)⁸⁸. However, in that study, only 42 glycan structures were detected, whereas we detected 52 *N*-glycans in our study. This is most likely due to a newer generation of MALDI mass spectrometer that provides improved ionisation and higher resolution detection capabilities. MALDI imaging also allowed for the validation of the results quantified previously by HILIC-UPLC, emphasising the significant differences seen previously upon LPS-injection.

Overall, the spatial changes observed in individual *N*-glycans through MALDI MSI are suggestive for the role of both individual structures and general glycosylation traits in the neuroinflammatory cascade, which is worth exploring further. In summary, the combination of these multifaceted glyco-analytical techniques allowed for a detailed, quantifiable and spatial characterisation of the *N*-glycophenotype in a reproducible and comprehensively described model of neuroinflammation. This provides a fair starting point for similar approaches to be taken in preclinical models of other brain conditions to decipher glycosylation's role on these.

Conclusions

This study presents the first step towards a deeper understanding of *N*-glycosylation's role in an LPS-induced model of neuroinflammation. A significant decrease in sialylation and fucosylation was seen upon LPS-injection, suggesting that this downregulation might play a crucial role as a potentiator of inflammatory cascades. An overall increase in oligomannose and bisected *N*-glycan structures seen in the inflamed tissue could indicate their involvement in this phenomenon as well. The use of a

combination of different glyco-analytical methodologies provides a complete knowledge of the brain's glycomic profiling, which opens avenues for further research to be done on this field.

Future studies focused on the regulation of glycosylation enzymes, on the expression of glycan-binding proteins (lectins) and on the glyco-profile of specific glycoproteins, will help to complete the molecular puzzle underlying this pathology and to further elucidate potential targets to be addressed in future therapies.

Abbreviations

[18F]DPA714 - [N,N-diethyl-2-(2-(4-(2-[18F]fluoroethoxy)phenyl)-5,7-dimethylpyrazolo[1, 5-a]pyrimidin-3-yl)acetamide]

BP_{ND} – Binding potential

CNS – central nervous system

dpi – days post-injection

GFAP – glial fibrillary acidic protein

HILIC-UPLC - hydrophilic interaction liquid chromatography – ultra-performance liquid chromatography

LPS – Lipopolysaccharide

MALDI MSI - Matrix assisted laser desorption ionisation mass spectrometry imaging

NI – non-injected

PD – Parkinson's disease

PET - Positron emission tomography

PSA – polysialic acid

TNF α - Tumour necrosis factor α

TSPO – 18kD Translocator protein

Vim - Vimentin

Declarations

Ethics approval and consent to participate

This study was carried out following European Union (Directive 2010/63/EEC) and French (Act Rural Code R214/87-131; authorisation no. B92-032-02) regulations and complied with Standards for Humane Care and Use of Laboratory Animals of the Office of Laboratory Animal Welfare (OLAW – n°A5826-01). All surgical procedures were reviewed and approved by the local ethics committee and registered with the French Research Ministry of Education and Research (committee no. 44, approval no. 12-100, APAFIS no. 389-20150327162135690v02).

Consent for publication

Not applicable

Availability of data and materials

All data generated and analysed during this study are available from the corresponding author on reasonable request.

Competing interests

The authors declare that they have no conflict of interests.

Funding Sources

This publication has emanated from research supported by a research grant from Science Foundation Ireland (SFI), co-funded under the European Regional Development Fund through Grant number 13/RC/2073 and by the BrainMatTrain project, which is funded by the European Union Horizon 2020 Programme (H2020-MSCA-ITN-2015) under the Marie Skłodowska-Curie Initial Training Network and Grant Agreement No. 676408. This work also benefited from support from the national "Infrastructure de recherche" NeurATRIS (Translational Research Infrastructure in Neurosciences, "Investissement d'Avenir", ANR-11-INBS-0011).

Authors' Contributions

A.L.R. performed all the experiments regarding *N*-glycan characterisation and analysis. F.G., P.R., N.V.C. and E.B. established the *in vivo* model and provided the animal tissue for the study. N.V.C. and P.R. performed and analysed the *in vivo* study. F.G. and P.R. performed the *post-mortem* pathological analysis of the LPS model and PBS-injected control. N.V.C. and E.B. managed and supervised the *in vivo* and *post-mortem* pathological analysis of the LPS model. C.J. carried out histological analysis of post-mortem tissues. R.R.D. managed and supervised the *N*-glycan characterisation using MALDI MS imaging. R.S. managed and supervised the *N*-glycan characterisation and analysis through liquid chromatography-based methods. A.P. conceptualised, supervised and managed the overall study. A.L.R. wrote the manuscript, which was reviewed, edited and approved by all co-authors.

Corresponding Author

Acknowledgments

The authors would like to acknowledge Mr Anthony Sloan and Dr Raghvendra Bohara for proof-reading this manuscript and Mr Maciej Doczyk for designing Figure 1. The authors are thankful to Mrs Pauline Gipchtein, Dr Marie-Claude Gaillard and Dr Martine Guillermier from MIRCen, Institut François Jacob, CEA (France) for their support in histology, qPCR and animal experimentation/PET imaging, respectively; and to Mrs Grace Grimsley from Medical University of South Carolina (USA) for her help in setting up the MALDI MSI experiments. The authors would like to thank also Dr Juhi Samal and Mr Kieran Joyce from CÚRAM, National University of Ireland Galway (Ireland) for their help with tissue collection procedures/experimental considerations, and assistance in *N*-glycan data interpretation, respectively.

References

- (1) Hirsch, E. C.; Hunot, S. Neuroinflammation in Parkinson's Disease: A Target for Neuroprotection? *Lancet. Neurol.***2009**, *8* (4), 382.
- (2) Krause, D. L.; Müller, N. Neuroinflammation, Microglia and Implications for Anti-Inflammatory Treatment in Alzheimer's Disease. *Int. J. Alzheimers. Dis.***2010**, *2010*, 732806.
- (3) Musella, A.; Gentile, A.; Rizzo, F. R.; Vito, F. De; Fresegna, D.; Bullitta, S.; Vanni, V.; Guadalupi, L.; Bassi, M. S.; Buttari, F.; Centonze, D.; Mandolesi, G. Interplay between Age and Neuroinflammation in Multiple Sclerosis: Effects on Motor and Cognitive Functions. *Front. Aging Neurosci.***2018**, *10*, 1.
- (4) Guzman-martinez, L.; Maccioni, R. B.; Andrade, V.; Navarrete, L. P.; Pastor, M. G.; Ramos-escobar, N. Neuroinflammation as a Common Feature of Neurodegenerative Disorders. *Front. Pharmacol.***2019**, *10*, 1.
- (5) Walker, D. G.; Yasuhara, O.; Patston, P. A.; McGeer, E. G.; McGeer, P. L. Complement C1 Inhibitor Is Produced by Brain Tissue and Is Cleaved in Alzheimer's Disease. *Brain Res.***1995**, *675* (1), 75.
- (6) Thomas, A.; Gasque, P.; Vaudry, D.; Gonzalez, B.; Fontaine, M. Expression of a Complete and Functional Complement System by Human Neuronal Cells in Vitro. *Int. Immunol.***2000**, *12* (7), 1015–1023.
- (7) Gasque, P.; Chan, P.; Mauger, C.; Schouft, M. T.; Singhrao, S.; Dierich, M. P.; Morgan, B. P.; Fontaine, M. Identification and Characterization of Complement C3 Receptors on Human Astrocytes. *J. Immunol.***1996**, *156* (6), 2247.
- (8) Walker, D. G.; Kim, S. U.; McGeer, P. L. Complement and Cytokine Gene Expression in Cultured Microglia Derived from Postmortem Human Brains. *J. Neurosci. Res.***1995**, *40* (4), 478.

- (9) Norden, D. M.; Godbout, J. P. Review: Microglia of the Aged Brain: Primed to Be Activated and Resistant to Regulation. *Neuropathol. Appl. Neurobiol.***2013**, *39* (1), 19.
- (10) DiSabato, D. J.; Quan, N.; Godbout, J. P. Neuroinflammation: The Devil Is in the Details. *J. Neurochem.***2016**, *139*, 136.
- (11) Laflamme, N.; Rivest, S. Toll-like Receptor 4: The Missing Link of the Cerebral Innate Immune Response Triggered by Circulating Gram-Negative Bacterial Cell Wall Components. *FASEB J. Off. Publ. Fed. Am. Soc. Exp. Biol.***2001**, *15* (1), 155.
- (12) Lehnardt, S.; Lachance, C.; Patrizi, S.; Lefebvre, S.; Follett, P. L.; Jensen, F. E.; Rosenberg, P. A.; Volpe, J. J.; Vartanian, T. The Toll-like Receptor TLR4 Is Necessary for Lipopolysaccharide-Induced Oligodendrocyte Injury in the CNS. *J. Neurosci.***2002**, *22* (7), 2478.
- (13) Shen, Y.; Qin, H.; Chen, J.; Mou, L.; He, Y.; Yan, Y.; Zhou, H.; Lv, Y.; Chen, Z.; Wang, J.; Zhou, Y.-D. Postnatal Activation of TLR4 in Astrocytes Promotes Excitatory Synaptogenesis in Hippocampal Neurons. *J. Cell Biol.***2016**, *215* (5), 719.
- (14) Acosta, C.; Davies, A. Bacterial Lipopolysaccharide Regulates Nociceptin Expression in Sensory Neurons. *J. Neurosci. Res.***2008**, *86* (5), 1077.
- (15) Chistyakov, D. V.; Azbukina, N. V.; Lopachev, A. V.; Kulichenkova, K. N.; Astakhova, A. A.; Sergeeva, M. G. Rosiglitazone as a Modulator of TLR4 and TLR3 Signaling Pathways in Rat Primary Neurons and Astrocytes. *Int. J. Mol. Sci.***2018**, *19* (1).
- (16) Kacimi, R.; Giffard, R. G.; Yenari, M. A. Endotoxin-Activated Microglia Injure Brain Derived Endothelial Cells via NF-KB, JAK-STAT and JNK Stress Kinase Pathways. *J. Inflamm. (Lond)***2011**, *8*, 7.
- (17) Park, B. S.; Lee, J.-O. Recognition of Lipopolysaccharide Pattern by TLR4 Complexes. *Exp. Mol. Med.***2013**, *45* (12), e66.
- (18) Bing, G.; Liu, M. Lipopolysaccharide Animal Models for Parkinson's Disease. *Parkinsons. Dis.***2011**, *2011*, 327089.
- (19) Zakaria, R.; Wan Yaacob, W. M.; Othman, Z.; Long, I.; Ahmad, A. H.; Al-Rahbi, B. Lipopolysaccharide-Induced Memory Impairment in Rats: A Model of Alzheimer's Disease. *Physiol. Res.***2017**, *66* (4), 553.
- (20) Batista, C. R. A.; Gomes, G. F.; Candelario-Jalil, E.; Fiebich, B. L.; de Oliveira, A. C. P. Lipopolysaccharide-Induced Neuroinflammation as a Bridge to Understand Neurodegeneration. *Int. J. Mol. Sci.***2019**, *20* (9), 2293.
- (21) Zhao, J.; Bi, W.; Xiao, S.; Lan, X.; Cheng, X.; Zhang, J.; Lu, D.; Wei, W.; Wang, Y.; Li, H.; Fu, Y.; Zhu, L. Neuroinflammation Induced by Lipopolysaccharide Causes Cognitive Impairment in Mice. *Sci. Rep.***2019**,

9 (1), 5790.

- (22) Catorce, M. N.; Gevorkian, G. LPS-Induced Murine Neuroinflammation Model: Main Features and Suitability for Pre-Clinical Assessment of Nutraceuticals. *Curr. Neuropharmacol.***2016**, *14* (2), 155.
- (23) Hunter, R. L.; Cheng, B.; Choi, D. Y.; Liu, M.; Liu, S.; Cass, W. A.; Bing, G. Intrastratial Lipopolysaccharide Injection Induces Parkinsonism in C57/B6 Mice. *J. Neurosci. Res.***2009**, *87* (8), 1913.
- (24) Deng, X.; Li, M.; Ai, W.; He, L.; Lu, D.; Patrylo, P. R.; Cai, H.; Luo, X.; Li, Z.; Yan, X. Lipolysaccharide-Induced Neuroinflammation Is Associated with Alzheimer-Like Amyloidogenic Axonal Pathology and Dendritic Degeneration in Rats. *Adv. Alzheimer's Dis.***2014**, *3* (2), 78.
- (25) Hoban, D. B.; Connaughton, E.; Connaughton, C.; Hogan, G.; Thornton, C.; Mulcahy, P.; Moloney, T. C.; Dowd, E. Further Characterisation of the LPS Model of Parkinson's Disease: A Comparison of Intra-Nigral and Intra-Striatal Lipopolysaccharide Administration on Motor Function, Microgliosis and Nigrostriatal Neurodegeneration in the Rat. *Brain. Behav. Immun.***2013**, *27* (1), 91.
- (26) *Essentials of Glycobiology*, Varki, A., Cummings, R. D., Esko, J. D., Freeze, H. H., Stanley, P., Bertozzi, C. R., Hart, G. W., Etzler, M. E., Eds.; Cold Spring Harbour Laboratory Press: New York, NY, 2009.
- (27) Apweiler, R.; Hermjakob, H.; Sharon, N. On the Frequency of Protein Glycosylation, as Deduced from Analysis of the SWISS-PROT Database. *Biochim. Biophys. Acta***1999**, *1473* (1), 4.
- (28) Helenius, A.; Aebi, M. Intracellular Functions of N-Linked Glycans. *Science (80-)***2001**, *291* (5512), 2364.
- (29) Kornfeld, R.; Kornfeld, S. Assembly of Asparagine-Linked Oligosaccharides. *Annu. Rev. Biochem.***1985**, *54*, 631.
- (30) Scott, H.; Panin, V. M. N-Glycosylation in Regulation of the Nervous System. *Adv. Neurobiol.***2014**, *9*, 367.
- (31) Jaeken, J.; Carchon, H. Congenital Disorders of Glycosylation: A Booming Chapter of Pediatrics. *Curr. Opin. Pediatr.***2004**, *16* (4), 434.
- (32) Rebelo, A. L.; Chevalier, M. T.; Russo, L.; Pandit, A. Sweet Tailoring of Glyco-Modulatory Extracellular Matrix-Inspired Biomaterials to Target Neuroinflammation. *Cell Reports Phys. Sci.***2021**, *2* (2), 100321.
- (33) Werneburg, S.; Mühlenhoff, M.; Stangel, M.; Hildebrandt, H. Polysialic Acid on SynCAM 1 in NG2 Cells and on Neuropilin-2 in Microglia Is Confined to Intracellular Pools That Are Rapidly Depleted upon Stimulation. *Glia***2015**, *63* (7), 1240.

- (34) Sumida, M.; Hane, M.; Yabe, U.; Shimoda, Y.; Pearce, O. M. T.; Kiso, M.; Miyagi, T.; Sawada, M.; Varki, A.; Kitajima, K.; Sato, C. Rapid Trimming of Cell Surface Polysialic Acid (PolySia) by Exovesicular Sialidase Triggers Release of Preexisting Surface Neurotrophin. *J. Biol. Chem.***2015**, *290* (21), 13202.
- (35) Demina, E. P.; Pierre, W. C.; Nguyen, A. L. A.; Londono, I.; Reiz, B.; Zou, C.; Chakraborty, R.; Cairo, C. W.; Pshezhetsky, A. V.; Lodygensky, G. A. Persistent Reduction in Sialylation of Cerebral Glycoproteins Following Postnatal Inflammatory Exposure. *J. Neuroinflammation***2018**, *15* (1), 336.
- (36) Paxinos, G.; Watson, C. *The Rat Brain in Stereotaxic Coordinates*, 4th ed.; Academic Press, 1998.
- (37) Kuhnast, B.; Damont, A.; Hinnen, F.; Catarina, T.; Demphel, S.; Le Helleix, S.; Coulon, C.; Goutal, S.; Gervais, P.; Dollé, F. [¹⁸F]DPA-714, [¹⁸F]PBR111 and [¹⁸F]FEDAA1106-Selective Radioligands for Imaging TSPO 18kDa with PET: Automated Radiosynthesis on a TRACERLab FX-FN Synthesizer and Quality Controls. *Appl. Radiat. Isot.***2012**, *70* (3), 489.
- (38) Lavisse, S.; Guillermier, M.; Hérard, A. S.; Petit, F.; Delahaye, M.; Van Camp, N. V.; Haim, L. Ben; Lebon, V.; Remy, P.; Dollé, F.; Delzescaux, T.; Bonvento, G.; Hantraye, P.; Escartin, C. Reactive Astrocytes Overexpress TSPO and Are Detected by TSPO Positron Emission Tomography Imaging. *J. Neurosci.***2012**, *32* (32), 10809.
- (39) Ichise, M.; Ballinger, J. R.; Golan, H.; Vines, D.; Luong, A.; Tsai, S.; Kung, H. F. Noninvasive Quantification of Dopamine D2 Receptors with Iodine-123-IBF SPECT. *J. Nucl. Med.***1996**, *37* (3), 513–520.
- (40) Cresto, N.; Gaillard, M. C.; Gardier, C.; Gubinelli, F.; Diguët, E.; Bellet, D.; Legroux, L.; Mitja, J.; Auregan, G.; Guillermier, M.; Josephine, C.; Jan, C.; Dufour, N.; Joliot, A.; Hantraye, P.; Bonvento, G.; Déglon, N.; Bemelmans, A. P.; Cambon, K.; Liot, G.; Brouillet, E. The C-Terminal Domain of LRRK2 with the G2019S Mutation Is Sufficient to Produce Neurodegeneration of Dopaminergic Neurons in Vivo. *Neurobiol. Dis.***2020**, *134*, 104614.
- (41) Samal, J.; Saldova, R.; Rudd, P. M.; Pandit, A.; Flaherty, R. O. Region-Specific Characterization of N-Glycans in Striatum and Substantia Nigra of an Adult Rodent Brain. *Anal. Chem.***2020**, *92*(19), 12842.
- (42) Küster, B.; Wheeler, S. F.; Hunter, A. P.; Dwek, R. A.; Harvey, D. J. Sequencing of N-Linked Oligosaccharides Directly from Protein Gels: In-Gel Deglycosylation Followed by Matrix-Assisted Laser Desorption/Ionization Mass Spectrometry and Normal-Phase High-Performance Liquid Chromatography. *Anal. Biochem.***1997**, *250* (1), 82.
- (43) Bigge, J. C.; Patel, T. P.; Bruce, J. A.; Goulding, P. N.; Charles, S. M.; Parekh, R. B. Nonselective and Efficient Fluorescent Labeling of Glycans Using 2-Amino Benzamide and Anthranilic Acid. *Anal. Biochem.***1995**, *230* (2), 229.

- (44) Royle, L.; Radcliffe, C. M.; Dwek, R. A.; Rudd, P. M. Detailed Structural Analysis of N-Glycans Released from Glycoproteins in SDS-PAGE Gel Bands Using HPLC Combined with Exoglycosidase Array Digestions. *Methods Mol. Biol.***2006**, *347*, 125.
- (45) Royle, L.; Campbell, M. P.; Radcliffe, C. M.; White, D. M.; Harvey, D. J.; Abrahams, J. L.; Kim, Y.-G.; Henry, G. W.; Shadick, N. A.; Weinblatt, M. E.; Lee, D. M.; Rudd, P. M.; Dwek, R. A. HPLC-Based Analysis of Serum N-Glycans on a 96-Well Plate Platform with Dedicated Database Software. *Anal. Biochem.***2008**, *376* (1), 1.
- (46) Angel, P. M.; Mehta, A.; Norris-Caneda, K.; Drake, R. R. MALDI Imaging Mass Spectrometry of N-Glycans and Tryptic Peptides from the Same Formalin-Fixed, Paraffin-Embedded Tissue Section. *Methods Mol. Biol.***2018**, *1788*, 225.
- (47) McDowell, C. T.; Klamer, Z.; Hall, J.; West, C. A.; Wisniewski, L.; Powers, T. W.; Angel, P. M.; Mehta, A. S.; Lewin, D. N.; Haab, B. B.; Drake, R. R. Imaging Mass Spectrometry and Lectin Analysis of N-Linked Glycans in Carbohydrate Antigen Defined Pancreatic Cancer Tissues. *Mol. Cell. Proteomics***2021**, *in press*, doi: 10.1074/mcp.RA120.002256.
- (48) Lu, X.; Zhang, D.; Shoji, H.; Duan, C.; Zhang, G.; Isaji, T.; Wang, Y.; Fukuda, T.; Gu, J. Deficiency of A1,6-Fucosyltransferase Promotes Neuroinflammation by Increasing the Sensitivity of Glial Cells to Inflammatory Mediators. *Biochim. Biophys. Acta - Gen. Subj.***2019**, *1863* (3), 598.
- (49) Powers, T. W.; Jones, E. E.; Betesh, L. R.; Romano, P. R.; Gao, P.; Copland, J. A.; Mehta, A. S.; Drake, R. R. Matrix Assisted Laser Desorption Ionization Imaging Mass Spectrometry Workflow for Spatial Profiling Analysis of N-Linked Glycan Expression in Tissues. *Anal. Chem.***2013**, *85* (20), 9799.
- (50) Nishikaze, T. Sensitive and Structure-Informative N-Glycosylation Analysis by MALDI-MS; Ionization, Fragmentation, and Derivatization. *Mass Spectrom.***2017**, *6* (1), A0060.
- (51) Wheeler, S. F.; Domann, P.; Harvey, D. J. Derivatization of Sialic Acids for Stabilization in Matrix-Assisted Laser Desorption/Ionization Mass Spectrometry and Concomitant Differentiation of $\alpha(2 \rightarrow 3)$ - and $\alpha(2 \rightarrow 6)$ -Isomers. *Rapid Commun. Mass Spectrom.***2009**, *23* (2), 303.
- (52) Kleene, R.; Schachner, M. Glycans and Neural Cell Interactions. *Nat. Rev. Neurosci.***2004**, *5* (3), 195.
- (53) Chang, I. J.; He, M.; Lam, C. T. Congenital Disorders of Glycosylation. *Ann. Transl. Med.***2018**, *6* (24), 477.
- (54) Furube, E.; Kawai, S.; Inagaki, H.; Takagi, S.; Miyata, S. Brain Region-Dependent Heterogeneity and Dose-Dependent Difference in Transient Microglia Population Increase during Lipopolysaccharide-Induced Inflammation. *Sci. Rep.***2018**, *8* (1), 2203.
- (55) Yao, R.; Pan, R.; Shang, C.; Li, X.; Cheng, J.; Xu, J.; Li, Y. Translocator Protein 18 KDa (TSPO) Deficiency Inhibits Microglial Activation and Impairs Mitochondrial Function. *Front. Pharmacol.***2020**, *11*,

- (56) Liddelow, S. A.; Guttenplan, K. A.; Clarke, L. E.; Bennett, F. C.; Bohlen, C. J.; Schirmer, L.; Bennett, M. L.; Münch, A. E.; Chung, W. S.; Peterson, T. C.; Wilton, D. K.; Frouin, A.; Napier, B. A.; Panicker, N.; Kumar, M.; Buckwalter, M. S.; Rowitch, D. H.; Dawson, V. L.; Dawson, T. M.; Stevens, B.; Barres, B. A. Neurotoxic Reactive Astrocytes Are Induced by Activated Microglia. *Nature***2017**, *541* (7638), 481.
- (57) Kim, Y. S.; Joh, T. H. Microglia, Major Player in the Brain Inflammation: Their Roles in the Pathogenesis of Parkinson's Disease. *Exp. Mol. Med.***2006**, *38* (4), 333.
- (58) Szepesi, Z.; Manouchehrian, O.; Bachiller, S.; Deierborg, T. Bidirectional Microglia–Neuron Communication in Health and Disease. *Front. Cell. Neurosci.***2018**, *12*, 323.
- (59) Holness, C. L.; Simmons, D. L. Molecular Cloning of CD68, a Human Macrophage Marker Related to Lysosomal Glycoproteins. *Blood***1993**, *81* (6), 1607.
- (60) Ory, D.; Planas, A.; Dresselaers, T.; Gsell, W.; Postnov, A.; Celen, S.; Casteels, C.; Himmelreich, U.; Debyser, Z.; Van Laere, K.; Verbruggen, A.; Bormans, G. PET Imaging of TSPO in a Rat Model of Local Neuroinflammation Induced by Intracerebral Injection of Lipopolysaccharide. *Nucl. Med. Biol.***2015**, *42* (10), 753.
- (61) Beier, E. E.; Neal, M.; Alam, G.; Edler, M.; Wu, L.-J.; Richardson, J. R. Alternative Microglial Activation Is Associated with Cessation of Progressive Dopamine Neuron Loss in Mice Systemically Administered Lipopolysaccharide. *Neurobiol. Dis.***2017**, *108*, 115.
- (62) Herrera, A. J.; Castaño, A.; Venero, J. L.; Cano, J.; Machado, A. The Single Intranigral Injection of LPS as a New Model for Studying the Selective Effects of Inflammatory Reactions on Dopaminergic System. *Neurobiol. Dis.***2000**, *7* (4), 429.
- (63) Han, L.; Zhang, D.; Tao, T.; Sun, X.; Liu, X.; Zhu, G.; Xu, Z.; Zhu, L.; Zhang, Y.; Liu, W.; Ke, K.; Shen, A. The Role of N-Glycan Modification of TNFR1 in Inflammatory Microglia Activation. *Glycoconj. J.***2015**, *32* (9), 685.
- (64) Kontou, M.; Weidemann, W.; Bork, K.; Horstkorte, R. Beyond Glycosylation: Sialic Acid Precursors Act as Signaling Molecules and Are Involved in Cellular Control of Differentiation of PC12 Cells. *Biol. Chem.***2009**, *390* (7), 575.
- (65) Quirico-Santos, T.; Fonseca, C. O.; Lagrota-Candido, J. Brain Sweet Brain: Importance of Sugars for the Cerebral Microenvironment and Tumor Development. *Arq. Neuropsiquiatr.***2010**, *68*, 799.
- (66) Isaev, D.; Isaeva, E.; Shatskih, T.; Zhao, Q.; Smits, N. C.; Shworak, N. W.; Khazipov, R.; Holmes, G. L. Role of Extracellular Sialic Acid in Regulation of Neuronal and Network Excitability in the Rat Hippocampus. *J. Neurosci.***2007**, *27* (43), 11587.

- (67) Yoo, S.-W.; Motari, M. G.; Susuki, K.; Prendergast, J.; Mountney, A.; Hurtado, A.; Schnaar, R. L. Sialylation Regulates Brain Structure and Function. *FASEB J.***2015**, *29* (7), 3040–3053.
- (68) Pshezhetsky, A. V.; Ashmarina, M. Keeping It Trim: Roles of Neuraminidases in CNS Function. *Glycoconj. J.***2018**, *35* (4), 375.
- (69) Kilcoyne, M.; Sharma, S.; McDevitt, N.; O’Leary, C.; Joshi, L.; McMahon, S. S. Neuronal Glycosylation Differentials in Normal, Injured and Chondroitinase-Treated Environments. *Biochem. Biophys. Res. Commun.***2012**, *420* (3), 616.
- (70) Zamze, S.; Harvey, D. J.; Chen, Y. J.; Guile, G. R.; Dwek, R. A.; Wing, D. R. Sialylated N-Glycans in Adult Rat Brain Tissue - A Widespread Distribution of Disialylated Antennae in Complex and Hybrid Structures. *Eur. J. Biochem.***1998**, *258* (1), 243.
- (71) Krusius, T.; Finne, J. Structural Features of Tissue Glycoproteins. Fractionation and Methylation Analysis of Glycopeptides Derived from Rat Brain, Kidney and Liver. *Eur. J. Biochem.***1977**, *78* (2), 369.
- (72) Cremer, H.; Chazal, G.; Goridis, C.; Represa, A. NCAM Is Essential for Axonal Growth and Fasciculation in the Hippocampus. *Mol. Cell. Neurosci.***1997**, *8* (5), 323.
- (73) Seki, T.; Arai, Y. Distribution and Possible Roles of the Highly Polysialylated Neural Cell Adhesion Molecule (NCAM-H) in the Developing and Adult Central Nervous System. *Neurosci. Res.***1993**, *17* (4), 265.
- (74) Nomura, T.; Yabe, T.; Rosenthal, E. S.; Krzan, M.; Schwartz, J. P. PSA-NCAM Distinguishes Reactive Astrocytes in 6-OHDA-lesioned Substantia Nigra from Those in the Striatal Terminal Fields. *J. Neurosci. Res.***2000**, *61*, 588.
- (75) Kiss, J. Z.; Wang, C.; Rougon, G. Nerve-Dependent Expression of High Polysialic Acid Neural Cell Adhesion Molecule in Neurohypophysial Astrocytes of Adult Rats. *Neuroscience***1993**, *53* (1), 213.
- (76) Shimizu, H.; Ochiai, K.; Ikenaka, K.; Mikoshiba, K.; Hase, S. Structures of N-Linked Sugar Chains Expressed Mainly in Mouse Brain. *J. Biochem.***1993**, *114* (3), 334.
- (77) Schneider, M.; Al-sharef, E.; Haltiwanger, R. S. Biological Functions of Fucose in Mammals. *Glycobiology***2017**, *27* (7), 601.
- (78) Fukuda, T.; Hashimoto, H.; Okayasu, N.; Kameyama, A.; Onogi, H.; Nakagawasai, O.; Nakazawa, T.; Kurosawa, T.; Hao, Y.; Isaji, T.; Tadano, T.; Narimatsu, H.; Taniguchi, N.; Gu, J. Alpha1,6-Fucosyltransferase-Deficient Mice Exhibit Multiple Behavioral Abnormalities Associated with a Schizophrenia-like Phenotype: Importance of the Balance between the Dopamine and Serotonin Systems. *J. Biol. Chem.***2011**, *286* (21), 18434.
- (79) Gu, W.; Fukuda, T.; Isaji, T.; Hang, Q.; Lee, H. H.; Sakai, S.; Morise, J.; Mitoma, J.; Higashi, H.; Taniguchi, N.; Yawo, H.; Oka, S.; Gu, J. Loss of A1,6-Fucosyltransferase Decreases Hippocampal Long

Term Potentiation: Implications for Core Fucosylation in the Regulation of AMPA Receptor Heteromerization and Cellular Signaling. *J. Biol. Chem.***2015**, *290* (28), 17566.

(80) Kalovidouris, S. A.; Gama, C. I.; Lee, L. W.; Hsieh-Wilson, L. C. A Role for Fucose Alpha(1-2)Galactose Carbohydrates in Neuronal Growth. *J. Am. Chem. Soc.***2005**, *9* (127), 1340.

(81) Nishihara, S.; Iwasaki, H.; Nakajima, K.; Togayachi, A.; Ikehara, Y.; Kudo, T.; Kushi, Y.; Furuya, A.; Shitara, K.; Narimatsu, H. Alpha1,3-Fucosyltransferase IX (Fut9) Determines Lewis X Expression in Brain. *Glycobiology***2003**, *13* (6), 445.

(82) Hennen, E.; Czopka, T.; Faissner, A. Structurally Distinct LewisX Glycans Distinguish Subpopulations of Neural Stem/Progenitor Cells. *J. Biol. Chem.***2011**, *286* (18), 16321.

(83) Satoh, J.; Kim, S. U. Differential Expression of Lewisx and Sialyl-Lewisx Antigens in Fetal Human Neural Cells in Culture. *J. Neurosci. Res.***1994**, *37* (4), 466.

(84) Kudo, T.; Fujii, T.; Ikegami, S.; Inokuchi, K.; Takayama, Y.; Ikehara, Y.; Nishihara, S.; Togayachi, A.; Takahashi, S.; Tachibana, K.; Yuasa, S.; Narimatsu, H. Mice Lacking Alpha1,3-Fucosyltransferase IX Demonstrate Disappearance of Lewis x Structure in Brain and Increased Anxiety-like Behaviors. *Glycobiology***2007**, *17* (1), 1.

(85) Regnier-Vigouroux, A. The Mannose Receptor in the Brain. *Int. Rev. Cytol.***2003**, *226*, 321.

(86) Harvey, D. J. Negative Ion Mass Spectrometry for the Analysis of N-Linked Glycans. **2019**, *39*, 586.

(87) Holst, S.; Heijs, B.; De Haan, N.; Van Zeijl, R. J. M.; Briaire-De Bruijn, I. H.; Van Pelt, G. W.; Mehta, A. S.; Angel, P. M.; Mesker, W. E.; Tollenaar, R. A.; Drake, R. R.; Bovée, J. V. M. G.; McDonnell, L. A.; Wuhrer, M. Linkage-Specific in Situ Sialic Acid Derivatization for N-Glycan Mass Spectrometry Imaging of Formalin-Fixed Paraffin-Embedded Tissues. *Anal. Chem.***2016**, *88* (11), 5904

(88) Eshghi, S. T.; Yang, S.; Wang, X.; Shah, P.; Li, X.; Zhang, H. Imaging of N-Linked Glycans from Formalin-Fixed Paraffin-Embedded Tissue Sections Using MALDI Mass Spectrometry. *ACS Chem. Biol.***2014**, *9* (9), 2149.

Figures

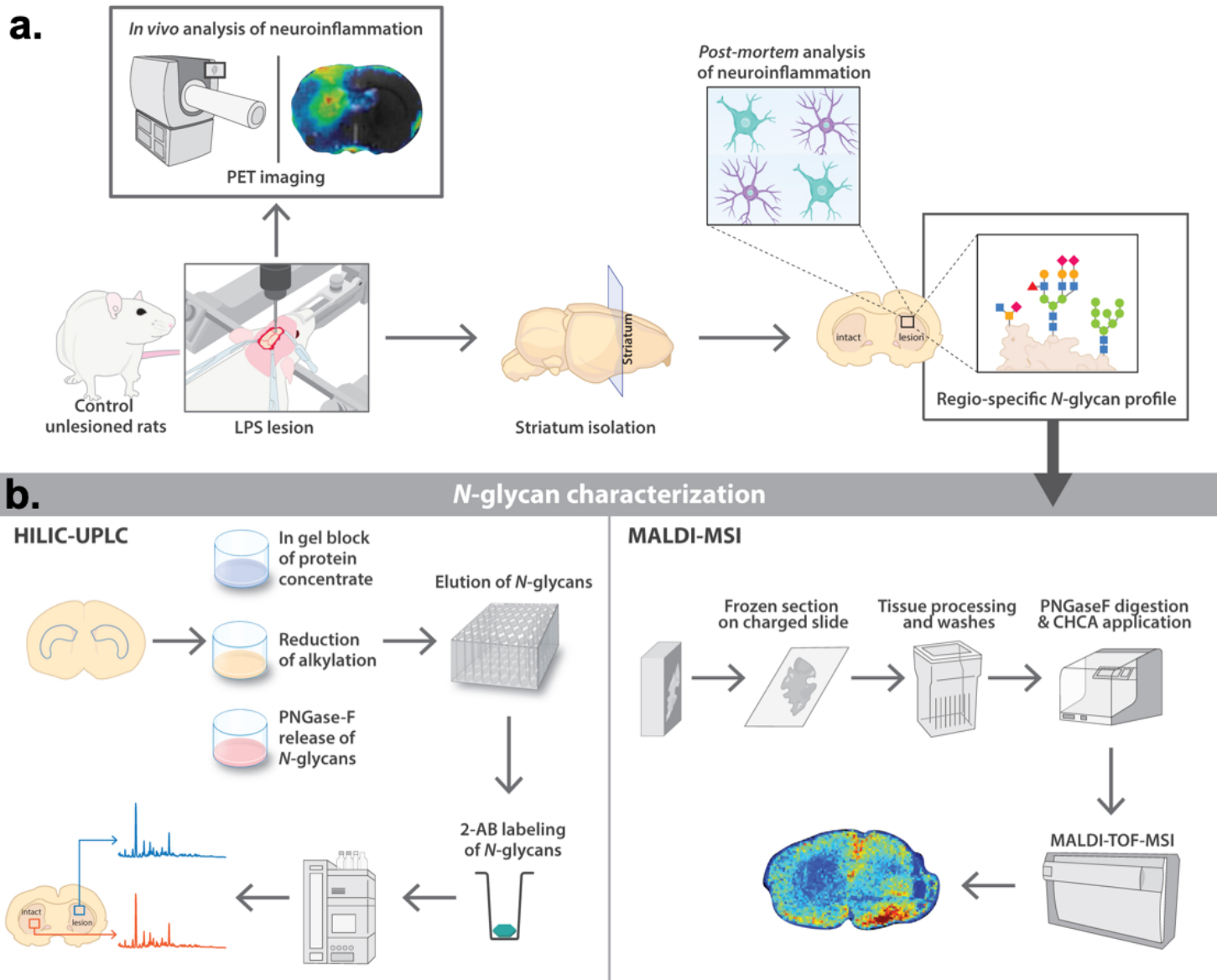
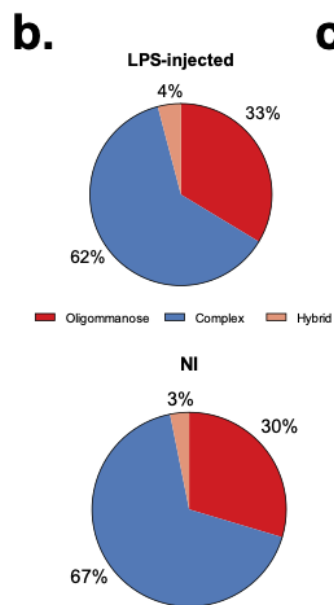
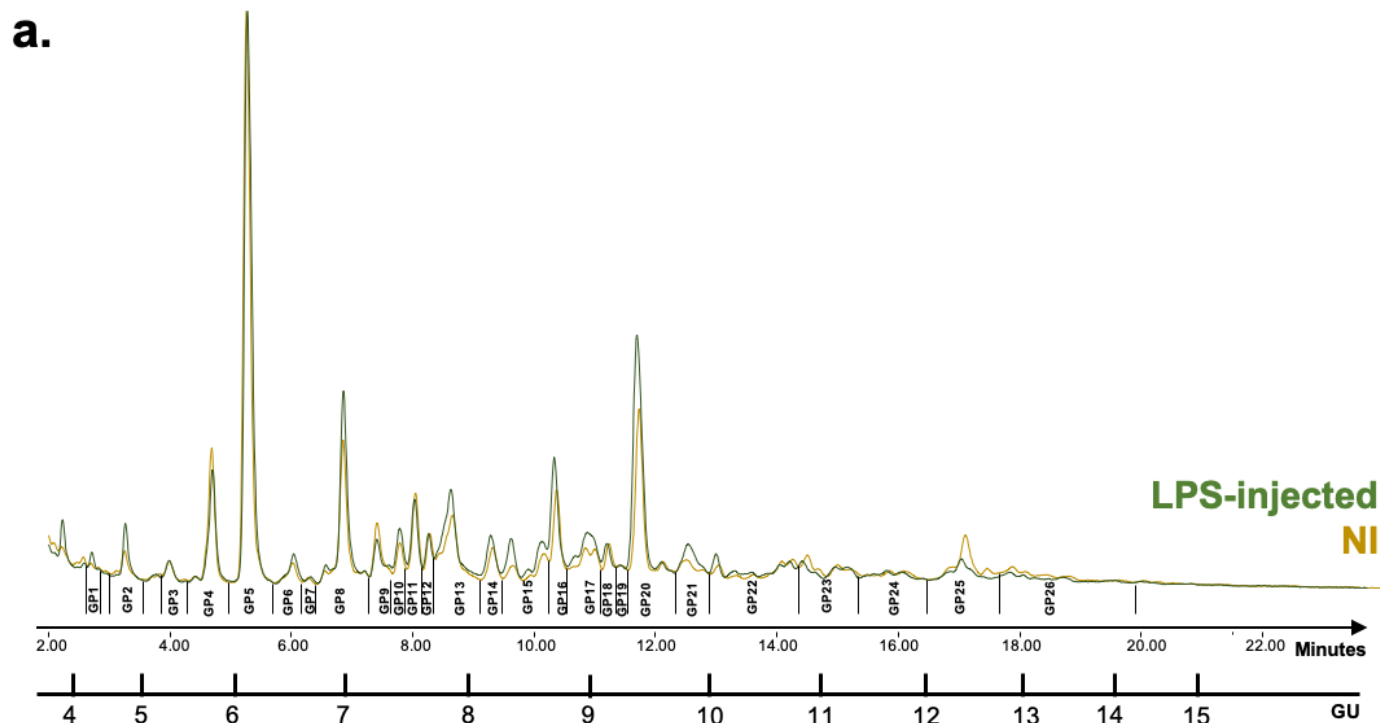


Figure 1



c.

	Composition	Structure	Significance	p value
GP1	M3		***	0.0009
GP2	M3B		***	0.0004
GP3	A1B		**	0.0050
GP4	FA2		**	0.0018
GP6	FA2G1		**	0.0020
GP9	FA2F1G1		**	0.0012
GP10	FA1BF1G1S2(3,8P)		**	0.0017
GP12	A2G2S1(6)Ac		*	0.0161

	Composition	Structure	Significance	p value
GP14	A2G2S1(3)		**	0.0036
GP15	FM5A1G1F1		***	0.0004
GP16	M8		*	0.0200
GP19	A2G2S2(3,6)		**	0.0057
GP20	M9		**	0.0016
GP21	A2F1G2S2(6,6)		**	0.0063
GP23	FA3F3G3		****	<0.0001
GP25	FA4F3G4S1(3)		***	0.0001

● Galactose
 ● Mannose
 ■ N-acetylglucosamine
 ▲ Fucose
 ◆ Sialic acid

Figure 2

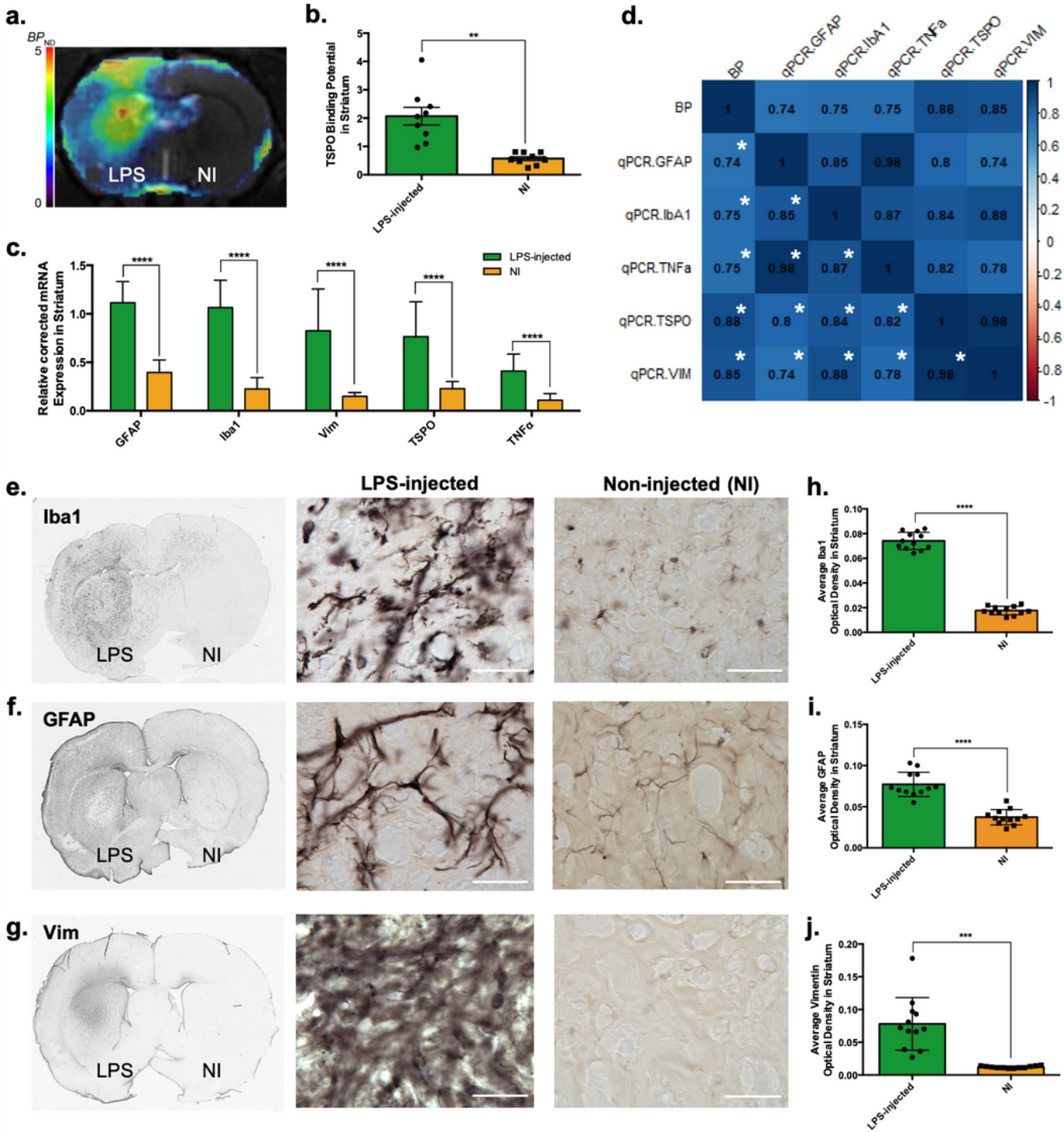


Figure 3

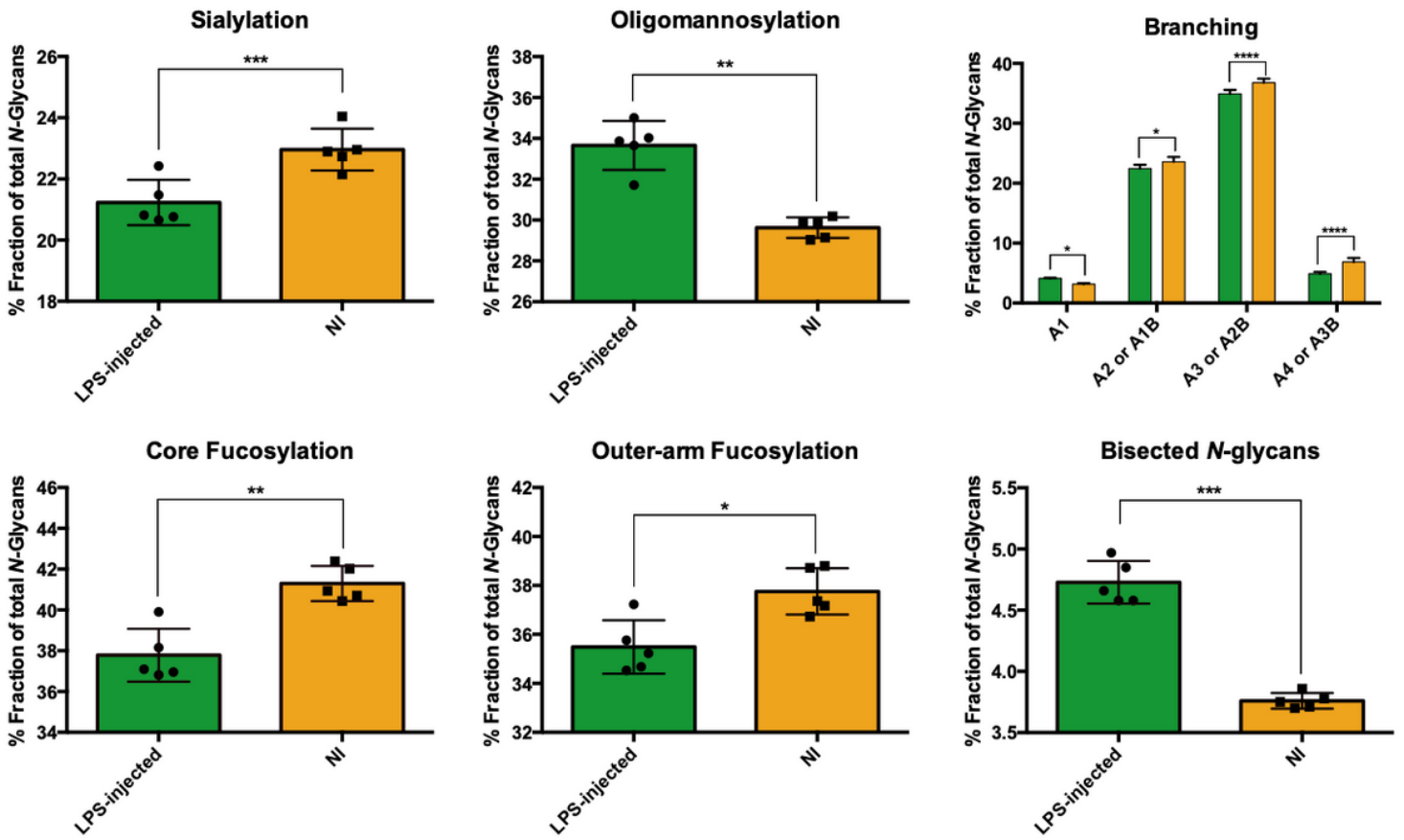


Figure 4

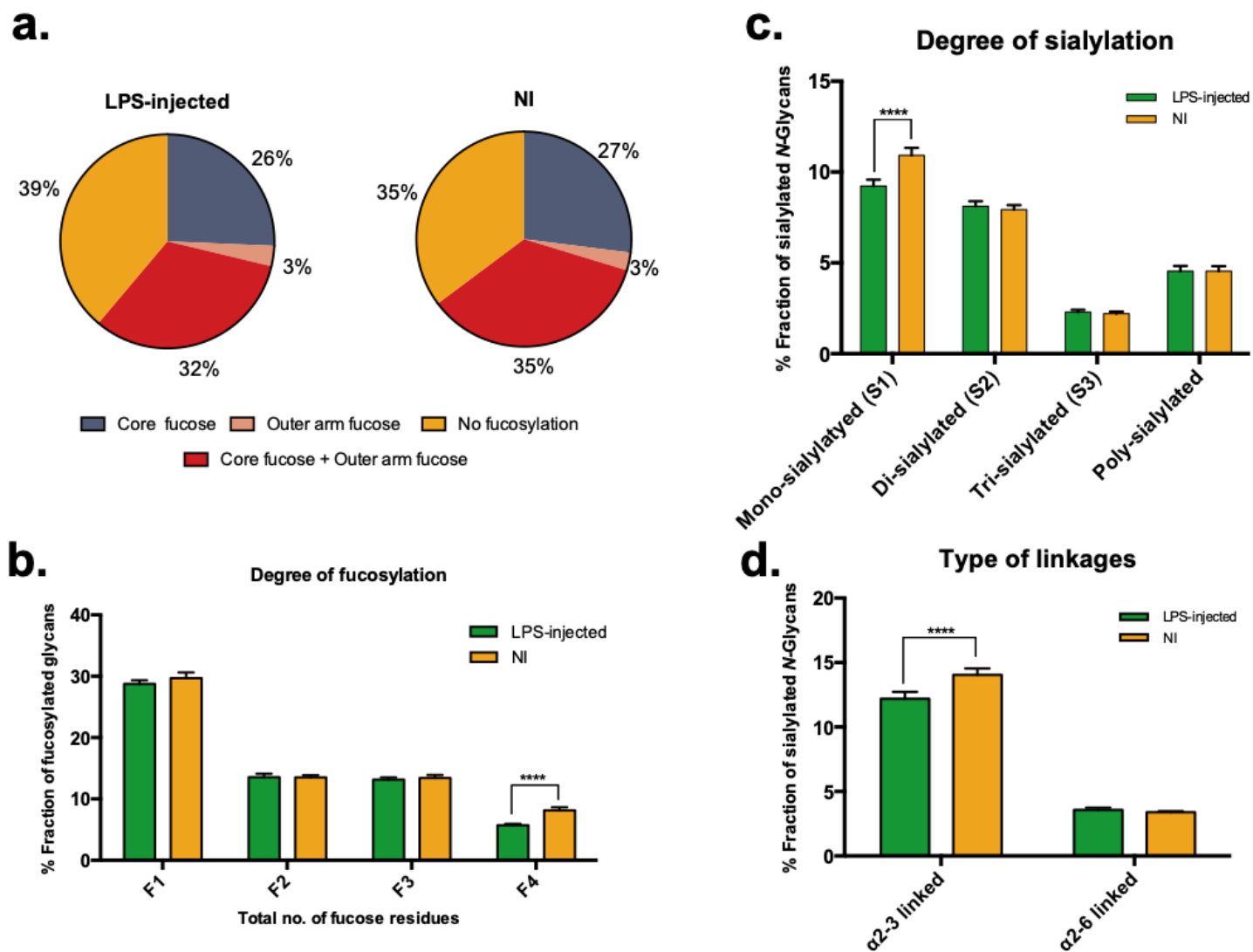


Figure 5

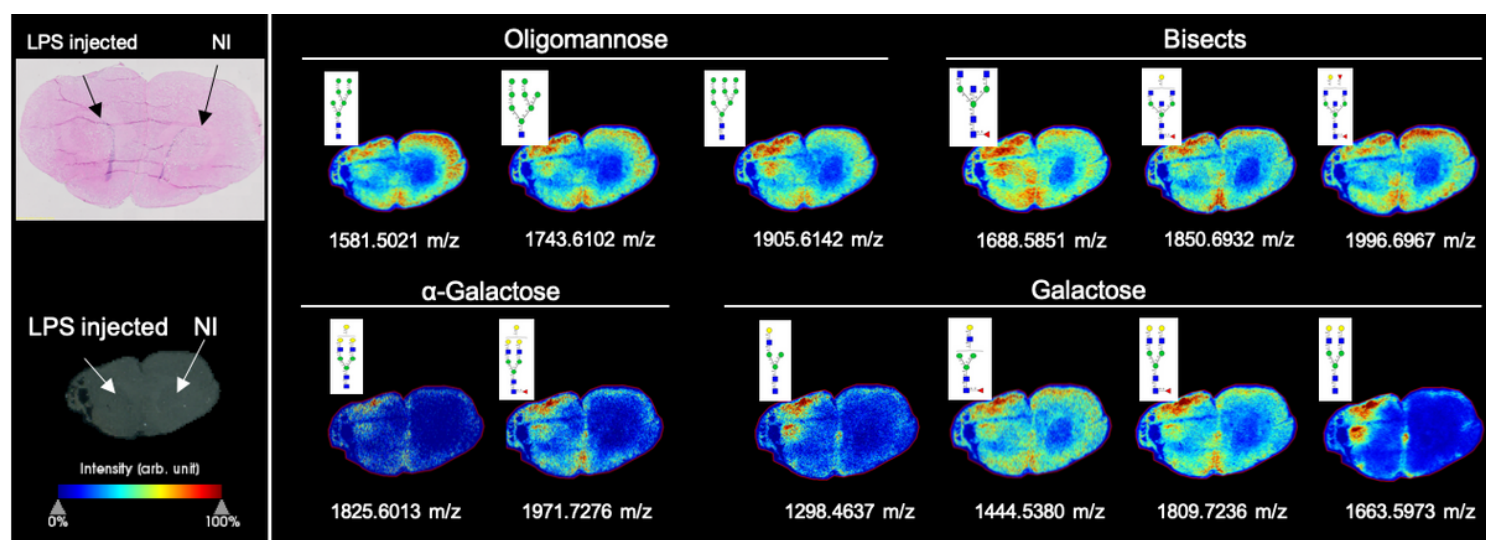


Figure 6

Supplementary Files

This is a list of supplementary files associated with this preprint. Click to download.

- [FigureS1.png](#)
- [FigureS2.png](#)
- [FigureS3.png](#)
- [FigureS4.png](#)
- [FigureS5.png](#)
- [equations.docx](#)